PHASE SEGREGATION STUDY OF

THERMOPLASTIC POLYURETHANES

A Thesis
Presented to
The Academic Faculty

by

Tamara Lee Mace

In Partial Fulfillment of the Requirements for the Degree
Master of Polymer Engineering

Georgia Institute of Technology

November 17, 2003

PHASE SEGREGATION STUDY OF THERMOPLASTIC POLYURETHANES

Approved:

Haskell Beckham, Chairman

Stephen Michielsen

Prashant Desai

Oomman Thomas

Hristo Hristov

Date Approved Nov. 24, 2003

DEDICATION

This work is dedicated to my family –

Charles, Noelle, and Justice for taking care of themselves and taking care of me too when times got crazy

My parents, Ron and Arlyn Cook – for always encouraging and supporting me in every way possible.

ACKNOWLEDGEMENT

Without the support of the following people I would never have been able to complete this body of work.

My coworkers and teammates – for being strong supporters especially Dr. Oomman Thomas for teaching me everything I needed to know and more. To Dr. Hristo Hristov for also teaching me so much. To Dr.Tom Mildenhall, Steve Englebert, Jon Wall, Keith Osteen, Cheryl Perkins and Cheri Everhart for believing I was worth the inconvenience to support this work.

Dr Ben Hsaio, Dr. Raj Somani, Dr. Carlos, Dr. Egors Sic..... and all of the people I worked with at both SUNY and Brookhaven National Lab.

For my research group at school- Swati Singla, Bryan White, Philip Watson, Kimberly Thompson, Teijun Zhao, Dr. Johannes Leisen, Toni Millikan, Craig Simile and Natasa Pajic- for all the patience and hours of emotional support, it sure was fun!! And of course Dr. Haskell Beckham for adopting me and putting up with the chaos long enough so that I could finish this work. Thank you.

TABLE OF CONTENTS

LIST OF FIGURES

LIST OF TABLES

LIST OF SYMBOLS

A_o	amplitude of incident wave
α	angle
a	Debye correlation length
Å	Angstrom
$\vec{b}$	scattered wave vector (Fourier space)
c	velocity of light in a vacuum
C_p	heat capacity
d	nearest neighbor spacing between domains
d	distance of electromagnetic wave with amplitude A_e
δ	phase angle
e	charge of electron
E'	storage modulus
E"	loss modulus
ε	strain
$\gamma(r)$	3-D correlation function
$\gamma(x)$	1-D correlation function
Inv.	SAXS Invariant
I	intensity
$\vec{k}$	scattering vector in Fourier space
l_c	coherence length
λ	Wavelength

m	mass of electron
N	number of electrons, number of particles, number of phase
ρ	electron density
Φ	volume fraction
R_g	radius of gyration
R^2	regression coefficient
s	scattering vector
σ	stress
v	path length
T_g	glass transition temperature
V	volume

SUMMARY

The phase segregation kinetics and evolution of domain morphology of two extruded thermoplastic polyurethane (TPU) polymers as a function time was studied using small angle x-ray scattering (SAXS). The two TPUs of similar molecular weight (200,000 Dalton) had the same type hard segments of 4,4'-diphenylmethane diisocyanate (MDI) chain extended with butane diol (BDO). The difference between the two polymers was the soft segment structure; one had an ether-based soft block and the other an ester-based soft block. The ether based soft block is polytetramethylene oxide (PTMO). The ester based soft block is poly-ε-caprolactone (PCL). The ether-based TPU (PTMO TPU) had a weight percent hard segment (MDI/BDO) of 24% and the ester-based TPU (PCL TPU) has a weight percent hard segment (MDI/BDO) of 39%.

In order to study the evolution of the domain morphology within seconds of extrusion, filaments were spun into a synchrotron x-ray beam path. The domain size and order in the first few seconds of extrusion were analyzed by the Debye method which assumes a random distribution, to obtain the hard segment interdomain spacing. This method was also used to analyze data generated for the PTMO TPU within minutes to days from extrusion. Similar analysis of the PCL TPU within minutes to days from extrusion could not be carried out because of the higher ordered nature of the domains. Vonk analysis yielded the hard domain size for the PCL TPU. Comparison of the two TPUs indicates that the PTMO TPU has a higher tendency to phase segregate than the PCL TPU and the domain size of the PCL TPU is larger than the PTMO TPU. In both polymers the

magnitude of the normalized relative invariant shows small changes up to 3.2 seconds from extrusion.

Effect of process quench temperature was observed by extruding the filaments onto either a room temperature roll (72°F) or a chilled roll (60°F). A relative invariant was used to measure the level of phase segregation in the polymers. Analysis of the PTMO TPU relative invariant data indicate that the filaments undergo different rates of segregation depending on the temperature of the casting roll. Analysis of the relative invariant data obtained for filaments extruded into the synchrotron beam, onto the chilled roll, and onto the room temperature roll fall on same line for the PCL TPU indicating that this system had the same rate of phase segregation independent of process conditions. The data obtained for the filaments extruded onto a room temperature roll combined with the synchrotron data showed a gradual change in the magnitude of the relative invariant for PTMO TPU, whereas the filaments extruded onto the chilled roll had a larger relative invariant. This implied that the PTMO TPU phase segregated better when extruded onto a chilled roll.

The effect of segregation on the properties of the filaments was also studied by differential scanning calorimetry (DSC), dynamic mechanical analysis (DMA), tensile and response to cyclic displacements. These data indicated that the TPUs were phase mixed within the first minutes of extrusion. Tensile data suggested that the phase segregation process occurring at a molecular level was not translated into the bulk properties of the filaments. Modulus, stress at yield and break did not show a trend with time from extrusion. Percentage set resulting from cyclic deformation, decreased as a function of time and phase segregation. Attempts to correlate changes in phase transitions measured by DMA to phase segregation did not yield meaningful results.

INTRODUCTION

Two types of elastomers are commercially available: a) thermoplastic and b) thermoset. Thermoplastic elastomers can be thermally processed while thermoset elastomers are cross-linked and cannot be thermally processed. The ability to thermally process a material and to reprocess the polymer provides options to design, develop, and commercialize new polymers and blends and can make materials which are recyclable.[1] Thermoplastic elastomers have several advantages over the original natural elastic materials. They do not require vulcanization and have relatively simple processing needs, just heat and pressure. The research work presented in this thesis relates to the study of the evolution of the morphology and mechanical properties of two segmented thermoplastic urethane elastomers.

Thermoplastic elastomers consist of at least two phases. These are designated as hard and soft phases. Figure 1a gives a model of an ideal two-phase thermoplastic elastomer system. The hard and soft phases segregate into hard domains within a continuous soft phase. The hard phase is normally rigid, amorphous or glassy, crystalline or semi-crystalline blocks whose purpose is to anchor the soft (rubber) blocks which would otherwise flow. By anchoring the soft blocks, the hard domains allow the soft blocks to stretch and retract without flowing or creeping. Figure 1b gives an example of a system with less phase segregation and less order. This model can be compared to a model of a covalently cross-linked network structure such as the structure shown in Figure 1d. The function of the hard domain in an elastomer is similar to that of the covalently bonded sulfur molecules which connect rubber molecules. The hard domains of an elastomer are not as robust as the covalent cross-links in holding the network

together. The inefficiency of the hard domain introduces additional rubber network defects which lead to inferior performing thermoplastic elastomers when compared to vulcanized rubber. The structure of a thermoplastic elastomer determines the behavior of the elastomer. Thermoplastic elastic block copolymers come in five main classes, with hard segments of styrenic, urethane, ether or amide. These block copolymers can have various soft segments such as ether or ester blocks among others.

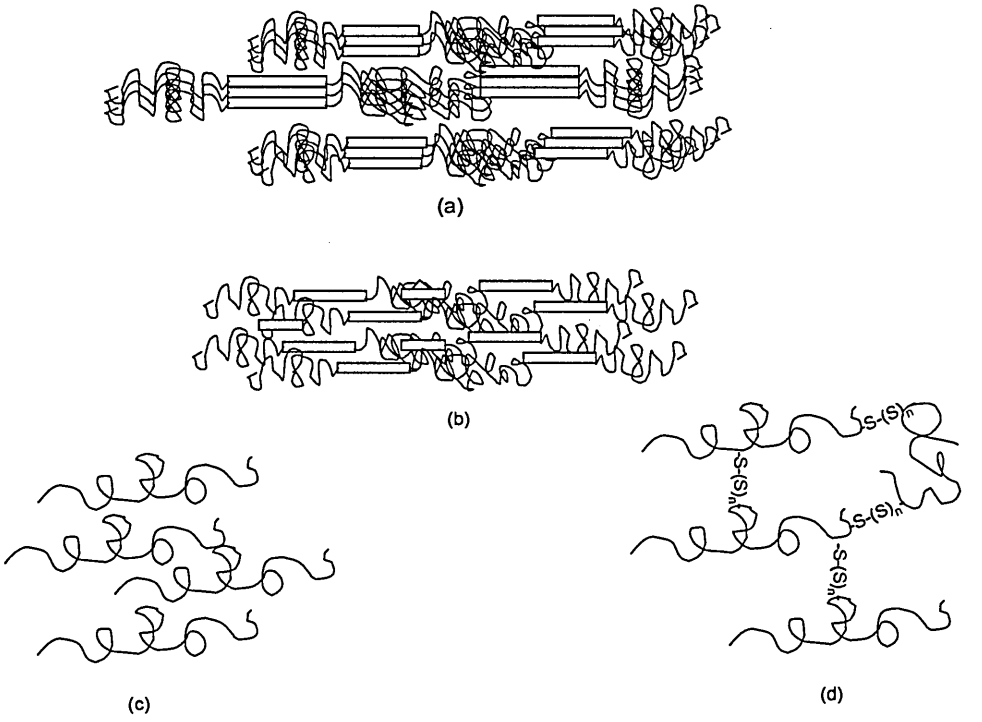

Figure 1. (a) schematic representation of a well phase segregated system (example Lycra Spandex, Kraton), (b) phase mixed system (example TPU), (c) non-vulcanized rubber molecules (natural rubber), and (d) sulfur vulcanized rubber molecules.

Generally the cost of an elastomer increases as the elastic performance it provides increases. One example of an elastomer that performs very well and is used both in disposable as well as durable product applications is Lycra Spandex. Lycra Spandex is a polyurea/urethane elastomer used in many applications because of its ability to retain elastic tension, i.e., it does not stress-relax over time under use

conditions such as diaper use. Specific applications of elastomers require different elastic behavior. One particular application is the elastic material in the side panel of Pull-Ups® disposable training pants sold by Kimberly-Clark Corporation. This material requires soft stretch tension with large elongation when the child is donning the pants and then is required to maintain a much smaller elongation with appropriate tension at body temperature during wear. Search for new or modified structures of existing elastomers to deliver desired performance continues to play an important role in the development of various consumer products. There are a myriad of types and varieties of thermoplastic elastomers and blends available that deliver low to high elastic performance. Examples of low-performance elastomers are plastomers based on ethylene and propylene chemistry. In these systems the hard phase consists of crystalline blocks and the soft phase consists of amorphous blocks of the polyethylene or propylene. The amorphous blocks can be created by copolymerizing olefin monomers with long side chains or by altering the stereochemistry.[2]

The difference between high-performance elastomers such as Lycra Spandex and styrenic block copolymers (SBC) derived from styrene block covalently bonded to blocks of saturated or unsaturated butadiene or isoprene rubber segment, compared to the plastomers above is that the hard blocks are mostly monodisperse and spontaneously segregate from the soft phase. This creates very uniform, phase segregated networks of hard segments interspersed in the soft continuous phase. This uniformity imparts excellent elastic stretch and recovery characteristics to the elastomer.

Most of the olefinic plastomers and many of the thermoplastic polyurethanes are sluggish in their phase segregation process and take minutes or even days to develop elastic properties. Although chemical modifications and or the addition of nucleating

agents can be implemented to change the speed of phase segregation, process conditions such as annealing can also be used to encourage speedy property development. This is particularly useful in a commercial process where the speed of conversion could be 2000 ft/min or more. If the elastic property does not develop in a few seconds, elastic laminate materials with stretch and recovery properties cannot be made.

An example of such a process is described in the United States patent No. 5,385,775 issued to Kimberly-Clark Corporation.[3] It is a process used to produce the elastic composite materials used in the side panel of the Pull-Ups® training pants. Figure 2 shows a schematic representation of the process. In this process the elastic filaments are extruded from a filament die and laid on a moving wire. The filaments are cooled immediately upon extrusion onto the wire and elastically stretched 5 to 6 times the original length through the stretch zone. The stretched filament sheet which enters the nip is then sandwiched between two spun bonded facings and allowed to retract as it leaves the nip roll. The relaxing step allows the laminate to retract and gather which provides elastic stretch properties. A type of elastomer that works very well in this process is the styrenic block copolymer.

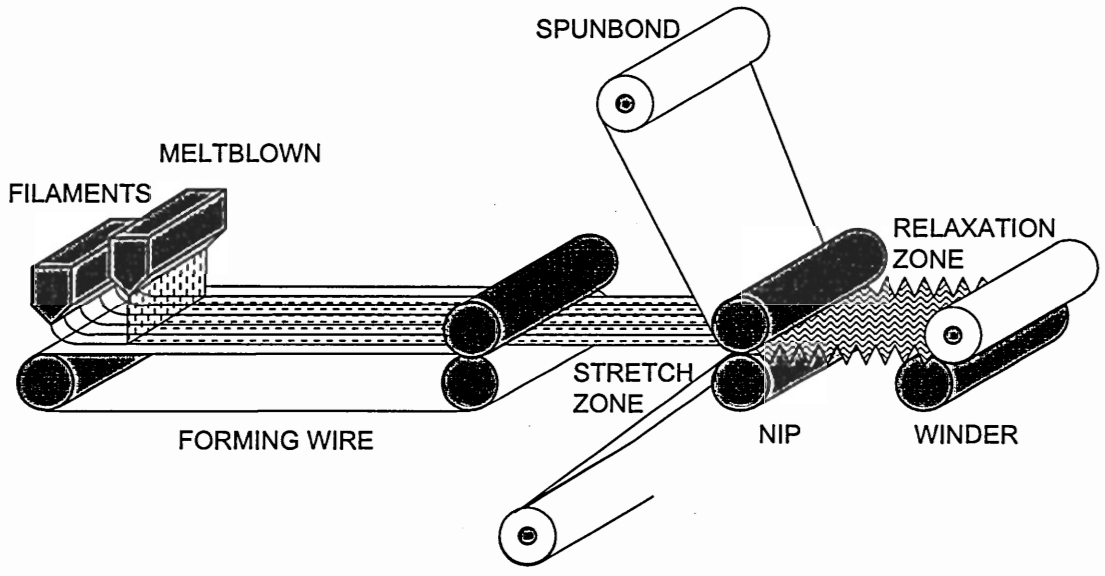

Figure 2. A schematic illustration of the elastic filament process used by Kimberly Clark Corporation to make Pull-Ups® side panel materials.

Attempts to use elastomers such as thermoplastic polyurethanes (TPU) to replace SBC polymers have resulted in materials with inadequate elastic stretch and recovery properties. TPUs do not develop elastic properties fast enough to be stretched and bonded to the facings to produce elastic laminate materials. One of the reasons for slow development of elastic properties is attributed to the inability of the hard phase to separate from the soft phase quickly. Several studies on the analysis of this problem have been conducted over the years such as those by Li, Gao, and Chu in 1991, and Li, Ren, Zhao, Yang and Chu in 1992.[4, 5] Given this problem and prior research in this area, the main objective of this study was to understand the time involved in the development of the domain morphology in two TPU elastomer systems. The development of domain morphology can be studied by morphological analysis as well as the evaluation of mechanical properties of the material. Thermoplastic polyurethanes are a very useful class if the polymer is allowed to age for a certain time after extrusion. The main

advantage of TPU polymers, when compared to styrenic block copolymers, is that they have higher moduli. The cost of a TPU is slightly higher than a styrenic block copolymer but, the TPU can deliver the same tension at a reduced weight of elastomer compared to a styrenic block thus creating an opportunity for cost savings.

TPUs are synthesized by combining two chemically dissimilar blocks, a soft polyol segment and hard segment of 4,4'-diphenylmethane diisocyanate (MDI) or toluene diisocyanate (TDI) or other isocyanate, that is chain extended with small molecule such as a diamine or a diol such as butane diol (BDO). The polyol block is referred to as the soft segment because, at room temperature, it is mobile and provides the stretching character. The hard segment at room temperature is in a rigid or glassy state. The coupling of the soft and hard blocks results in a general structure $-(S—H))_n—$. The weight percentage of hard and soft segment in the copolymer, along with the chemical structure, controls the elastic properties of the copolymer. An example of the chemical structure of the hard segment of the two polymers chosen for this study is shown in Figure 3. The first polymer chosen has a poly-ε-caprolactone (PCL) soft segment that is an ester. The second polymer chosen has the same hard segment but a polytetramethylene oxide (PTMO) soft segment. These two polymers were chosen because of their commercial significance as well as structural dissimilarities. The TPU polymer made using PTMO is known to phase segregate better and faster than the polymer that contains the poly-ε-caprolactone (PCL) soft segment. The objective of this study was to understand how the elastic properties develop after extrusion in these two systems as a function of time.

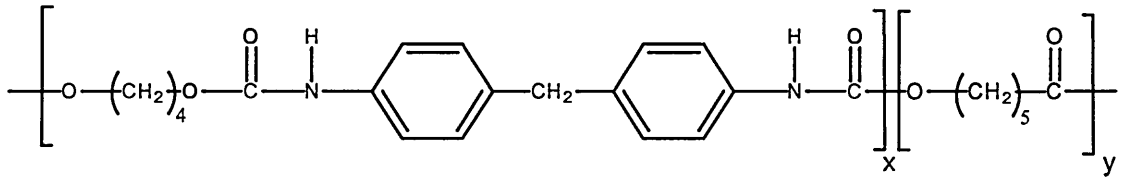

a)

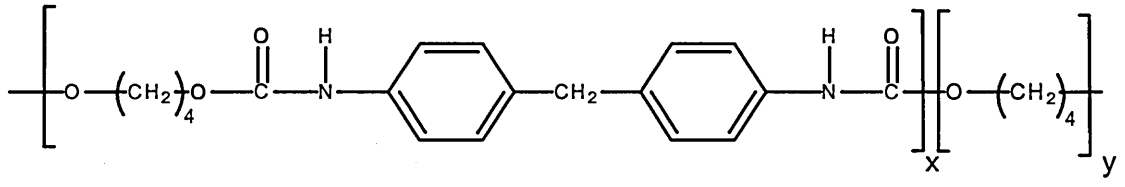

b)

Figure 3. a) Chemical structures of the TPU hard segment with the PCL soft segment. b) Chemical structure of the TPU hard segment with the PTMO soft segment.

One of the tools used extensively in the study of evolution of the hard phase morphology of copolymers is small angle x-ray scattering (SAXS). One can study the formation of domains by spinning a filament of interest into the x-ray beam path and using SAXS methods. To capture the evolution of the domain in real time, the x-ray beam has to be intense. One such source of intense x-rays is the synchrotron radiation source available at Brookhaven National Laboratory (BNL) in New York. Excellent accounts of the use of SAXS to study the structure/property relationship in many phase segregated elastomer systems have been published by various authors.[6, 7]

A good understanding of the effects of chemical structure, hard segment content, and processing conditions, on the evolution of domain morphology, rate of phase segregation, and the development of physical properties of the two TPU systems are necessary for this study. Cooper and Velankar (1998) studied the phase separation of polyurethane melts as a function of hard block length using SAXS.[8] Three key variables

that control the structure and properties of the TPU were defined: hard and soft block lengths, hard and soft block incompatibility, and composition.

Chu, Gao, and Li (1991) studied the phase separation kinetics of a segmented polyurethane with synchrotron SAXS.[4] This study assessed the effect of annealing temperature on the phase separation rate of a PTMO soft segment TPU with an MDI/ BDO hard segment based TPU. They found an optimal annealing or quench temperature for the fastest rate of phase segregation above which the compatibility of the hard and soft segments increases. The Chu study concluded that below the optimal temperature conditions, phase separation rate and level is reduced. Chu concludes that this reduction is due to a decrease in kinetics, therefore lack of sufficient chain mobility. Above the optimal temperature the rate was reduced because of thermodynamics increasing compatibility between the hard and soft segments. A physical blend was compared with the covalently bonded block copolymer system and found to phase separate much faster than the latter. The covalent bonding in the block copolymer is thought to have also contributed to the slow phase segregation process. The kinetics of a block copolymer are hindered compared to a physical blend. These findings may explain why the TPU systems are slow to phase segregate in general.

Chu et al (1992) also studied the phase structure of segmented polyurethanes as a function of hard segment flexibility using synchrotron SAXS analysis to assess the effects of thermodynamics vs. kinetics during the phase segregation of TPUs.[5] Using the value of the relative invariant from the SAXS analysis and the soft segment T_g observed by differential scanning calorimetry (DSC), it was found that increased hard segment content did not increase the phase segregation of the system. This finding does not match with the theory that predicts higher hard segment content leads to lower

compatibility between the soft and hard phases, which should promote segregation. This unexpected behavior was explained by Chu et al as a function of kinetics.

Koberstein et al (1992) and Cooper et al (1998)[9,8] have studied TPUs based on poly-ε-caprolactone soft segment and MDI/BDO hard segment. In order to study the effect of hard block size on morphology, Koberstein et al. chose the poly-ε-caprolactone soft segment because of its miscibility with the hard segment. A range of block lengths showed that this compatibility level combined in polymers with smaller block lengths showed no phase segregation as indicated by SAXS analysis. The short hard block lengths are thought to dissolve into the soft phase for these types of systems. At increasingly larger block lengths, the position of the SAXS peak indicates phase segregation but only of short range order. This is explained as a morphology that has short-term order in the form of lamellar hard segment regions dispersed in the soft continuous phase. As the distance increases from a hard segment, the correlation does not continue past a few stacks of lamella. The normalized relative invariant is used as a way to quantify the level of phase segregation in these systems because the scattering plots do not show higher order peaks.

Koberstein and Leung (1992) studied the microphase segregation in compression-molded TPUs by measuring and comparing the soft segment T_g through DSC analysis.[11] They reported that the glass transition behavior of the TPU was more complex than could be explained by simple thermodynamics. The complex transition behavior was attributed to the effects of hydrogen bonding and physical crosslinking as well as some amount of hard segment dissolved in the soft phase. Koberstein and Galambos et al (1992) also studied the correlations between the thermal/

thermomechanical properties and the microdomain structure of thermoplastic polyurethane.[9] DSC characterization of the urethane systems as a function of hard segment content showed the existence of multiple endotherms for systems with less than 40% hard segment. They describe the morphology of the systems with less than 40% hard segment as having discrete hard domain structure in a continuous phase of soft segment. Koberstein et al also indicate that systems with higher percent hard segment show a better drive to segregate. Koberstein's finding does not agree with Chu's findings from a study done at the same time.[8]

Pompe et al (1997) studied the influence of processing conditions on the multiphase structure of segmented polyurethanes.[10] They identify the development of at least two types of hard segment crystallites during the processing of the TPU. The process temperature impacts the content of type I and II hard segment crystallites. The findings of the study indicate that the mechanical properties of the TPU can be controlled by choosing processing temperature ranges that correlate to a specific morphology. This study directly links the phase segregation level and specific morphology to the mechanical properties of the TPU.

Like any other copolymer the mechanical properties of TPUs are a function of their domain morphology and level of phase segregation. An example of a study on linking properties and morphology was done by Harrell (1969), where the change in physical properties of a TPU was studied as a function of segment size and their distribution in the polymer.[12] The study assessed the effect of hard and soft segment sizes and their distribution as well as the spacing along the polymer molecule. The study included thermal properties and mechanical properties such as stress-elongation and percent set determination of the TPUs. The degree of crystallinity did not vary with

segment size. The soft segment size distribution was found to greatly impact the physical properties of the TPU. Narrowing of the soft segment size distribution showed an increase in modulus and elongation properties as well as increasing extension set properties.

The present study will include the collection and analysis of SAXS data on in-situ spun TPU filaments as well as filaments as they age. Two polymers are considered with two different soft segments at differing levels of hard segment but the same hard segment type. The study will consider the effect of percentage hard segment and the type of soft segment on the phase segregation process. The effect of quench temperature during processing on phase segregation kinetics is also assessed. A normalized relative invariant is used to quantify the level of phase segregation in these systems since the scattering plots do not show higher order peaks. The magnitude of the normalized relative invariant is used to quantify the phase segregation level as filaments age in the current study. A comparison will be made to relate the specific morphology and level of phase segregation as measured by SAXS analysis to the DMA, hysteresis and tensile properties of the TPU systems. The current study will also include analysis of the soft segment T_g as measured by DSC. The glass transition of a pure soft segment polymer can be compared to the glass transition of the soft segment in a copolymer to assess the level of phase mixing in the system. If hard segments are mixed into the soft segments then the glass transition temperature will increase due to stiffening. The current study includes assessment of the effect of aging time and quenching temperature on the glass transition temperature of the two TPUs studied.

EXPERIMENTAL

Materials

The two TPU polymers chosen for this study were kindly provided by Dow Chemical of USA. They are sold under the trade name Pellethane^{R} and designated by code numbers 2102-80 A and 2103-70A. The 2102-80A will be referred to as the PCL TPU and 2103-70A will be referred to as the PTMO TPU. Table 1 shows the soft segment molecular weight, and the weight percentage of hard segment of these two polymers. The molecular weight data furnished by Dow Chemical indicates that both polymers have comparable overall molecular weight of the order of 200,000 g/mole.[13]

Table 1. Soft segment molecular weight, and weight percentage of hard segment of the two TPU polymers of this study

Soft Segment (SS)	Soft Segment Molecular Weight (Daltons)	Hard Segment Content (Wt %)
Polycaprolactone	2000	39
Polytetramethylene Oxide	2000	24

Methods

Brabender Filament Extrusion To study the post spinning and long-term development of morphology, filament samples of the TPU polymers were made on a Brabender IntelliTorque plasti-corder rheometer equipped with a three-zone single

metering screw. The compression ratio of the screw was 2.5/1 and the L/D ratio was 24/1. The screw has three heating zones; the feed zone (50% of the length of the screw) and two metering zones (each 25% of the length of the screw). In addition, the extruder is fitted with a filament die that can be heated. The filament was extruded at a back pressure of 600 – 1000 psi at 20 rpm. Polymer in the form of pellets was introduced in the hopper of the extruder and the temperature of the screw zones and the die and the screw RPM were adjusted such that a filament of desired properties was obtained. The extruded filament upon exiting the die was passed onto either a chilled roll or a room temperature roll and finally to a windup roll whose speed was adjusted to get a filament with very low draw.

Table 2 Brabender extrusion set-up at Kimberly Clark Corp. for filament extrusion

Polymer	Temperatures °C				Pressure at die (psi)	Torque (Meter x grams)
	feed zone	2nd zone	3rd zone	Die		
PTMO TPU	180	200	210	210	400	2200
PCL TPU	180	200	210	220	400	2300

Filament Extrusion at Brookhaven National Laboratory The same TPU polymers were used to produce filaments at Brookhaven National Laboratory (BNL) at the advanced polymer beamline X27C at the National Synchrotron Light Source (NSLS). A picture of the extrusion system is shown in Figure 4.[14]

Filaments of the TPU polymers were obtained using a melt index (MI) apparatus equipped with a 0.375 inch diameter heated barrel and a motor driven plunger moving at

0.11 inches /minute which extruded the polymer through a die at the bottom of the barrel. The diameter of the die used for the filament extrusion was 0.75 mm. This MI apparatus was placed on top of a platform which could be moved vertically over a distance of about 100 mm with a 0.2 mm precision, allowing the detection spot along the spin line to be changed. The apparatus was mounted on a pair of precision optical rails perpendicular to the X-ray beam, which permits the alignment of the filament with the x-ray beam. The extruded filament was directed to a room temperature roll 254 mm below which also controlled the filament movement during exposure to x-ray beam. A take up roll was placed beside the chill roll and the filament was wound up. All the experiments were performed at ambient temperature (25°C).

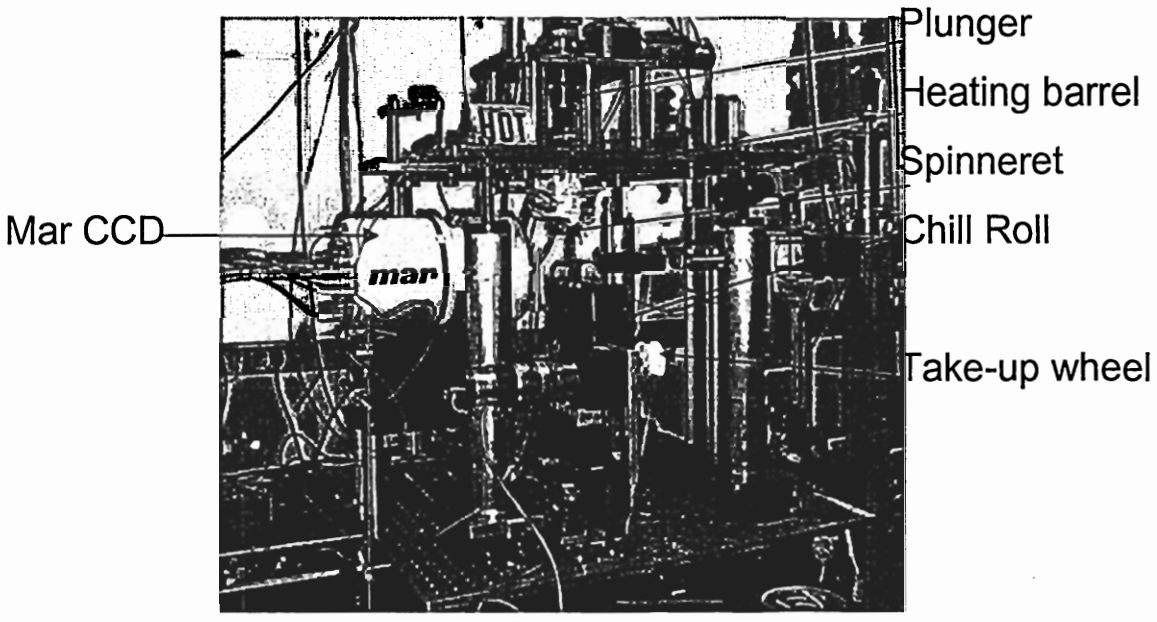

Figure 4. A picture of the filament extrusion set up at Brookhaven National Labs on the Advanced Polymer Beamline X27C.[15]

Solution- Cast Films To study the equilibrium structure thin TPU film samples were made by solution casting and slow cooling. The solution cast films were produced by dissolving the polymer pellets in tetrahydrofuran (THF). The solvent-solute mixture

was heated to 60°C in a microwave oven and stirred to dissolve the polymer pellets into a 20% solution. The solution was then poured into aluminum trays and allowed to cool in a hood. The aluminum trays were then placed in an oven under vacuum for three days at room temperature to form films of the polymer as the volatile THF evaporated.

Compression-Molded Films Compression-molded films of the PCL based TPU were produced to study the morphology. The films were made by heating a Carver press top and bottom platen to 220°C and placing a small amount of the polymer pellets in between the platens in a 2" diameter x 1/8" circular space created by shim material. The platens were brought together at 50 psi and held together for 2 minutes. The pressure was released and the platens turned off, which allowed the sample to cool very slowly to room temperature. Table 3 gives the detailed description of sample preparation for various measurements under different conditions.

Table 3. Description of processing types and conditions for all samples produced and studied

Location	Process Type	Equipment Used	Process Details	Heat Profile	Pressure
Kimberly-Clark Corp. Roswell GA	Solution-casting	aluminum pans, fume hood, microwave and vacuum oven	used THF to dissolve TPU's	60°C in microwave, room temperature for cooling,	N/A
Kimberly-Clark Corp. Roswell GA	Compression-molding	Carver press with heated platens	used shims to control film thickness	220°C slow cooled	50 psi on platen
Kimberly-Clark Corp. Roswell GA	filament extrusion	Brabender intellitorque rheometer	single screw extruder with filament die and chill roll at 62°F	180°C to 220°C	400 psi die pressue
Brookhaven National Lab	filament extrusion	melt index apparatus with 3/4" barrel and driven plunger		220°C	N/A

SAXS Measurements

SAXS Measurements at Kimberly Clark Corp. in Roswell SAXS measurements were performed on the samples from the Brabender extrusion process as well as the solution-cast and compression-molded samples at Kimberly Clark Corporation in Roswell, Georgia on an X-ray diffractometer manufactured by Inel Inc. To collect data in the small angle range (SAXS), the instrument is equipped with a linear position-sensitive detector (LPS-50) covering the angular interval of 0.1° to 6°. This angle would correspond to a long spacing range from 800 to 15 Å. The specimens were irradiated with CuK_α monochromatic radiation (wavelength λ = 0.1542 nm) by eliminating the CuK_β line using a Ni filter in the primary beam. The SAXS data were collected in

transmission geometry at time intervals ranging from 10 to 120 minutes (the exposure duration used was sufficient to provide scattering data with low statistical error). The "standard" collection time was 60 minutes for the true intensity curve and the background/air scattering. The beam length was limited (quasi-pinhole collimation) so no desmearing of the data was necessary.

SAXS Measurements at Brookhaven National Labs The real-time data acquisition to study the evolution of domain morphology of the TPUs at very short times from extrusion was carried out on the synchrotron x-ray source at BNL. Synchrotron SAXS experiments were completed on the Advanced Polymer Beamline X27C at the NSLS. A schematic of the SAXS set-up is shown in Figure 5.[14] This beamline consists of a high precision pinhole system that is suitable for SAXS studies. The X-ray beam was collimated through a three pinhole system (190 cm long) with the last pinhole size being 0.37mm in diameter. The beam was aligned with the filament and each sample was exposed for between 1 and 2 minutes. The distance between the detector and the sample was calculated to be 1437 mm. Further details of the SAXS equipment and set-up can be found in previous work published by Chu et al.[15]

In order to obtain the development of morphology as a function of time it was necessary to expose the filament to the beam at various locations. This was accomplished by moving the stage up and down along the z-direction of the filament. A schematic representation of the positions at which the filaments were exposed is shown in Figure 6.

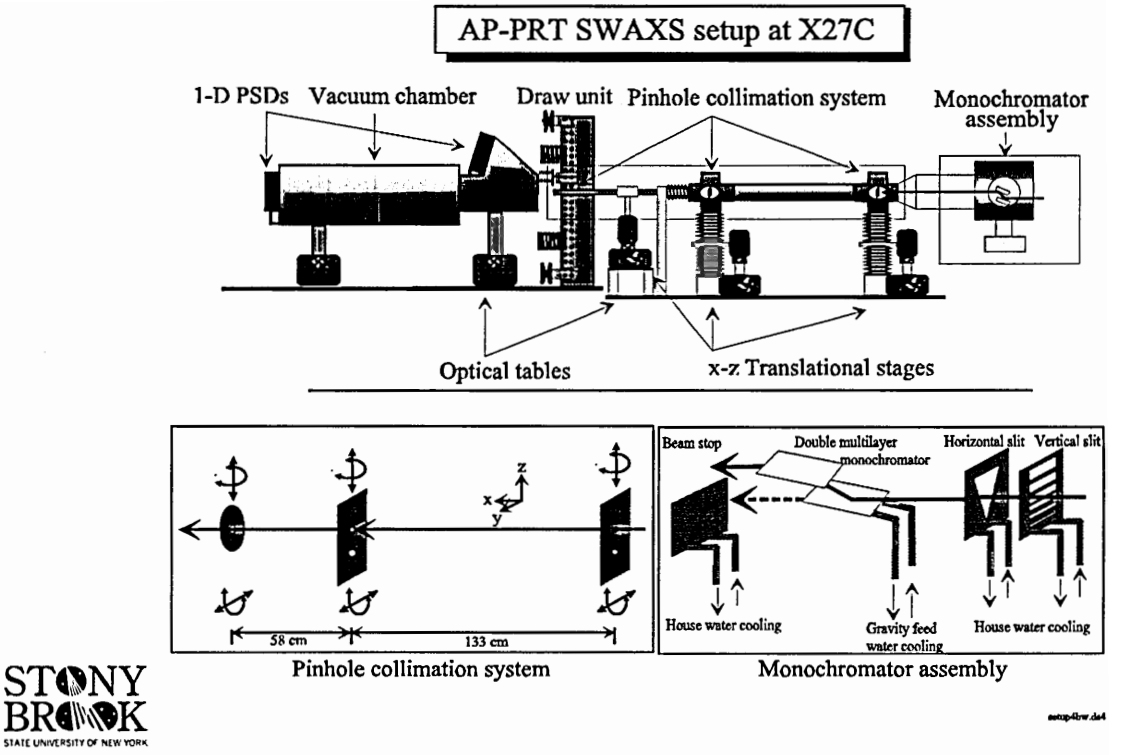

Figure 5. The SAXS set-up at BNL advanced polymer beamline X27C

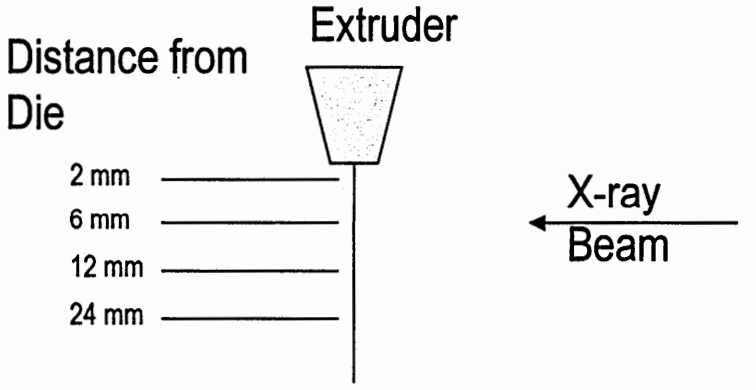

Figure 6. A drawing of the beam to filament set up at BNL for in-situ spinning experiments. Extruder is raised and lowered to image the extruded filament at a specific distance from the die.

Theory of SAXS

SAXS is a method by which structural features of the order of 15-2000 Å in size may be studied. X-rays are scattered by the electrons of a sample and the amplitude of the scattering radiation is given by the three-dimensional Fourier transformation of the electron-density distribution. Analysis of the intensity as a function of angle reveals valuable information about the morphology of the material. SAXS technique can be used to analyze dilute or dense systems. Below are the theoretical approaches in both cases.

The polymers studied here are physically dense systems in that they are solid polymers, but it is possible that the phase segregation proceeds only in a few locations. Thus, the system could be considered as a combination of dilute scatterers in a continuous matrix of phase-mixed polymer.

Scattering of X-Rays by an Electron When an electromagnetic wave of electric field amplitude A_0 interacts with an electron of charge, *e*, and mass, *m*, the electron undergoes an acceleration given by A_0e/m.[6] The accelerating electron then radiates an electromagnet wave whose amplitude A_e at a distance *d* is given by:

$$A_e = \frac{e\sin\alpha}{dc^2} * \frac{A_0 e}{m} = \frac{A_o e^2 \sin\alpha}{dmc^2} \qquad (1)$$

where α is the angle between the incident beam and the electron acceleration vector, and c is the speed of light. However, the intensity of a wave is the square of its amplitude, then it follows that

$$I_e = \frac{e^4 \sin^2 \alpha}{d^2 m^2 c^4} I_o \tag{2}$$

where I_o and I_e are the intensities of the incident and scattered beams. If the incident beam is unpolarized, the intensity of the scattered beam can be given by Thompson's rule:

$$I_e = I_o \left[\frac{1}{d^2}\right]\left[\frac{e^4}{m^2 c^4}\right]\left[\frac{1+\cos^2 2\theta}{2}\right] \tag{3}$$

where 2θ is the angle between the scattered and incident beam.[6] This equation describes the elastic scattering where the incident and scattered waves have the same wavelength. When the scattered waves coming from each electron are produced by the same incident wave, there exists a relationship between the phases which produces an x-ray diffraction pattern. Inelastic collisions between photons and electrons result in scattered waves of different wavelength do not yield meaningful x-ray diffraction patterns.[7]

Interference and Diffraction of Scattered X-rays To analyze the scattered intensity resulting from a group of electrons, the amplitude of the scattering of each electron must be considered; these are summed and the result squared. This summing consists of constructive as well as destructive interference which results in a pattern that is characteristic of the electron density distribution in the sample. The total intensity scattered by a group of electrons depends only on the group of electrons and is independent of their arrangement. The spatial arrangement only affects the intensity as a function of the scattering angle.

Assume that a collection of electrons is irradiated by a plane wave traveling in the direction of a unit vector, $\vec{b}_0$, with a wavelength of λ. The intensity of the scattered beam in the direction of $\vec{b}$, can now be determined. If the amplitude A of a wave front scattered by an electron at an origin in a volume defined by N electrons is given by:

$$A = A_e e^{-2\pi i v} \tag{4}$$

where A_e is the amplitude of the electric field scattered by the electron and ν is the distance from the x-ray source to the observation point in wave numbers. If the position of the j^{th} electron is defined by a vector, $\mathbf{x}_j$, from an origin, O, to the i^{th} electron, then the path length difference between the incident wave front at the origin and the position of the i^{th} electron is given by:

$$\frac{-\left(\vec{b}_0 \bullet \vec{x}_j\right)}{\lambda} \tag{5}$$

The path length difference between the scattered wave front at the origin and at the position of the i^{th} electron is given by:

$$\frac{+\left(\vec{b}_0 \bullet \vec{x}_j\right)}{\lambda} \tag{6}$$

The total path length difference between the path through the origin and through the i^{th} electron is:

$$\frac{\vec{b}\bullet\vec{x}_j}{\lambda}-\frac{\vec{b}_0\bullet\vec{x}_j}{\lambda}=\vec{x}_j\bullet\frac{(\vec{b}-\vec{b}_0)}{\lambda} \tag{7}$$

The scattering vector, $\vec{s}$, is then defined as $\frac{(\vec{b}-\vec{b_0})}{\lambda}$

Then the path length difference for the i^{th} electron is given by

$$v_j=\vec{s}\bullet\vec{x}_j \tag{8}$$

See Figure 7 for an illustration of the scattering of x-ray by a group of electrons (represented by 1,2 and 3).[7]

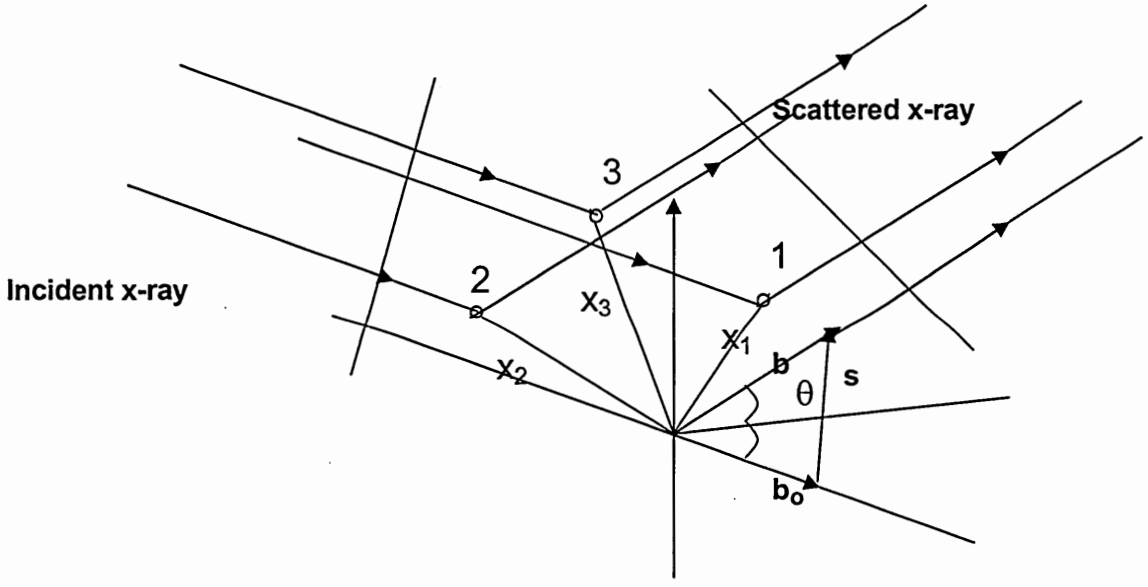

Figure 7. Schematic representation of x-ray beams scattered by electrons as described by Kakudo.[7]

Equation 4 can then be rewritten as

$$A = A_e e^{-2\pi i \vec{s} \bullet \vec{x}_j} \tag{9}$$

The relationship between the amplitude of radiation scattered by a substance and its morphology is reflected in the distribution of its electron density. The total intensity for all the electrons at s would be the summation of Equation 9 over all electrons. In integral form it can be expressed as:

$$A(\vec{s}) = A_e(\vec{s}) \int_v \rho(x) \exp[-2\pi i(\vec{s}\vec{x})\overrightarrow{dx} \tag{10}$$

As shown in Figure 7 the angle between the vectors $\mathbf{b}_o$ and $\mathbf{b}$ is 2θ. A(s) is the amplitude of the scattered radiation at s, $\rho(x)$ is the electron density distribution within the sample and A_e is the amplitude of a single electron. This equation gives the Fourier transformation of the electron density distribution within the sample.[18] The scattering angle between the incident and the scattered beam is 2θ. The length of the scattering vector is given by:

$$s = |\vec{s}| = \frac{2\theta}{\lambda} \tag{11}$$

The intensity of the scattering is then given by the conjugate product of the scattering amplitude[4], i.e.,

$$I(\vec{s}) = I_e(\vec{s})[\int_V \rho(x) \exp^{[-2\pi i(k \bullet x)]}\, dx]^2 \tag{12}$$

For computational purposes it convenient to introduce a scattering vector $\vec{k} = 2\pi\vec{s}$.

$$k = |\vec{k}| \equiv \frac{4\pi \sin\theta}{\lambda} \cong \frac{4\pi\theta}{\lambda}$$

For a single electron, the above expression can be written as:

$$I_e(k) = \left[\frac{I_o}{d^2}\right]\left[\frac{1+\cos^2 2\theta}{2}\right]7.90x10^{-30}m^2 \qquad (13)$$

where I_o represents the intensity of the incident beam , d the distance in meters between the sample and the detector and $e^4/m^2c^4=7.90x10^{-30}$ meter^2 is know as the Thompson factor. Hence the scattering curve is a reciprocal or Fourier space representation of the real space morphology.

Experimental data suffers from polychromatic radiation, parasitic scattering, smearing, and background scattering. Appropriate filters are used to ensure a monochromatic beam. Desmearing of the beam is ensured by using pinhole geometry. The edges of the collimating slits and the air can cause parasitic scattering. Hence the scattering obtained in absence of the sample is subtracted from the scattering with the sample in place. Statistical density fluctuation or background within the sample must also be corrected. Analysis of the data can then be carried out.

Analysis of the Dilute System In dilute systems the interparticle scattering can be neglected and the scattering intensity only reflects the intraparticle scattering. In such

systems, particle size in terms of the radius of gyration can be obtained by Guinier's approximation.[16]

$$I(k) = \left(\frac{Nm^2}{V}\right)\exp^{\left(-4p^2k^2R_g^{\frac{2}{3}}\right)} \quad (14)$$

Where I is the intensity of the scattering, N represents the number of scattering particles, m is the mass, V is the volume of particles, k is the scattering vector and R_g represents the radius of gyration of the scattering particle.

Another parameter related to the particle size introduced by Porod is the coherence length l_c, which is given by[19,20,21]

$$l_c = 0.5\frac{\int_0^\infty k\ I(k)dk}{\int_0^\infty k^2 I(k)dk} \quad (15)$$

As one increases the concentration of the particles secondary maxima related to interparticle interference (diffraction) will appear.

Analysis Of Dense Two-Phase Systems Increasing the number of scatterers leads to interparticle interference and the analysis of the sample morphology requires assumptions regarding the structure. To extract the characteristics of the morphology, several approaches can be used. The types of analysis used for a very regular structure, such as a lamellar aggregation and for a completely random structure are discussed below. This analysis will show that the structures of the TPUs studied fall between the extremes of an ordered lamellar structure and a completely random structure.

1-Dimensional Correlation Function

In an arrangement of domains in a lamellar aggregation and assuming that in random locations, the orientation of the lamellae is random, it is appropriate to use the Vonk 1D correlation function.[6,22]

$$\gamma_{1D}(x) = \frac{\int_0^\infty k^2 I(k) \cos x \quad kdk}{\int_0^\infty k^2 I(k) dk} \tag{16}$$

where x is the axis perpendicular to the layers of the lamella. A schematic illustration of the general shape of this function is shown below in Figure 8.

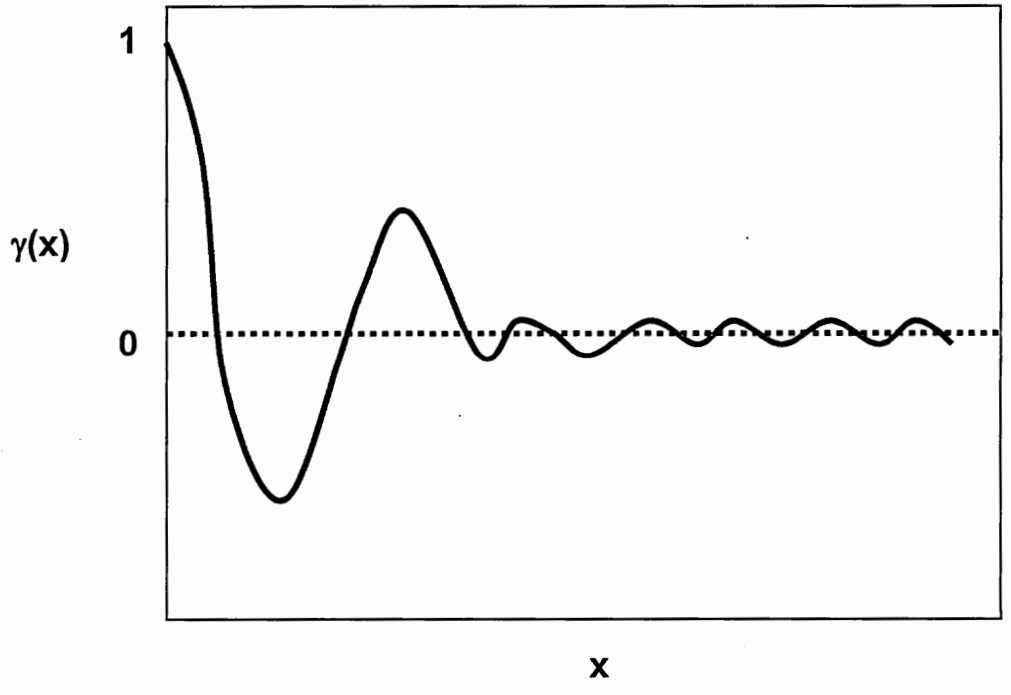

Figure 8. A schematic illustration of a 1-dimensional correlation function of a lamellar structure according to Vonk.

The distance between lamella can be obtained by the location of the maximum in the correlation function. This number is the average interdomain spacing for the system being considered.

Debye Method

The Debye method assumes that scattering particles have a significant variation in their size and/or shape and are completely randomly oriented.[22] In the case of a random structure the correlation function among the scatterers is given by Equation 17:

$$\gamma(\mathrm{r}) = e^{(-\mathrm{r}/\mathrm{a})} \tag{17}$$

The function is one dimensional due to the randomness of the system. The Fourier image of a structure described by a random aggregation of particles is given by:

$$\mathrm{I(k)} = \mathrm{Constant} \Big/ (1 + \mathrm{k}^2\mathrm{a}^2)^2 \tag{18}$$

where *a* is the Debye correlation length. The value of *a* is then obtained from a plot of

$\frac{1}{\sqrt{\mathrm{I(k)}}}$ vs. k^2, where the value of *a*, the correlation length; is given by

$$[a = \left(\mathrm{slope} \Big/ \mathrm{intercept}\right)^{\frac{1}{2}}] \tag{19}$$

In a dense two-phase structure the size of the hard domains can be computed from:[12]

$$l_H = \frac{a}{\phi_H} \tag{20}$$

where Φ_H is the volume fraction of the hard segment in the polymer.

Degree of Phase Separation

The intensity of the scattering curve is related to the degree of phase separation via the invariant. The invariant is related to the mean square electron density difference within a material, $\overline{\Delta\rho^2}$.[22] For a two-phase system with phases A and B, with sharp phase boundaries, this value is given by the electron density of each phase and their corresponding volume fractions as:

$$\overline{\Delta\rho^2} = \Phi_A \Theta_B (\rho_A - \rho_B)^2 \qquad (21)$$

Absolute determination of $\overline{\Delta\rho^2}$ [(electrons/unit volume)^2] requires knowledge of the intensity in electron units $I_e(k)$ which requires an absolute measure of the incident beam intensity I_o. Incident beam intensity can be determined by the use of a standard scattering sample such as Lupolene.[6]

The quantity: [21]

$$\text{Inv} = \int_0^\infty k^2 I(k) dk = \frac{1}{V} \int_V \rho(r) * \rho(r + \Delta r)\ dV \qquad (22)$$

is known as the invariant. For a material containing a specific set of atoms, the invariant does not change regardless of morphological changes, as long as the integral is taken over the entire diffraction space. On SAXS scale (distances from 15 to 2000 angstroms), the scattering approaches zero in homogeneous materials. Presence of concentration differences ($\Delta\rho$ not zero) will result in development of SAXS patterns. The shape and the intensity of the patterns depend on the specific morphology. This intensity and its

distribution are measured in the course of the SAXS experiments. In such cases the integral in Equation 23 is a measure of the concentration differences in the SAXS range, thus a measure of the overall phase segregation.

$$\text{Inv} = \int_0^{k_{max}} k^2 I(k) dk = \frac{1}{V} \int_V \Delta\rho^2 dV \qquad (23)$$

The upper limit of the integral in Equation 23 is usually less than 1 Angstrom^{-1}. The invariant approach is valid in dilute and concentrated systems.

SAXS Data Calibration and Correction

Figure 9 shows a 2-D side-by-side plot of the scattering pattern of the two TPU filaments as they exited the die at a distance of 2 mm and were exposed to the synchrotron x-ray beam. The streaks seen along the equator on the two images can be attributed to the presence of micro voids developed during the spinning process. These streaks are small but intense and indicate the existence of voids oriented parallel to the filament axis. The intensity at low scattering angle is very high implying that the difference in electron density between the scattering particles (the voids) and the matrix is very large. The effect on the intensity at smaller angle is further illustrated in Figure 10 in a I-D plot of the equatorial and meridional scattering patterns.

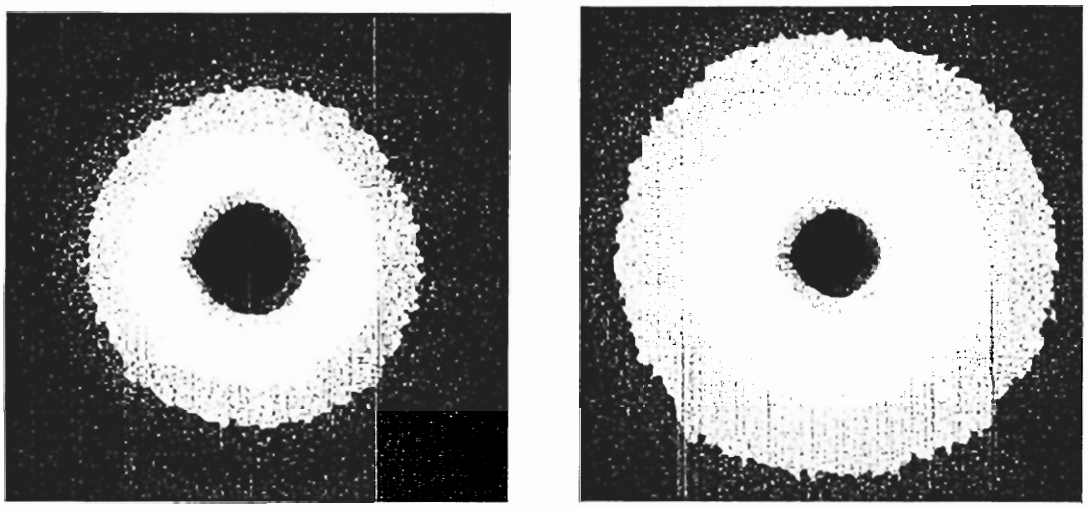

{a} {b}

Figure 9. 2-D scattering images from BNL advanced polymer beamline SAXS (a – PCL TPU b – PTMO TPU both at 2 mm from extruder)

The analysis of the data therefore must take into account the presence of these streaks. The data can be corrected for the streak which affects a small region at very small angles. In order to maximize the quality of the scattering data for analysis, an azimuthal scan was performed after the streak was removed from the image by eliminating the intensity data for pixels with levels lower than 25. The azimuthal averaging gives the advantage of improved statistics. Because the statistical error is proportional to 1/sqr(N) where N is the number of scattering entities, the statistical error can be reduced significantly when an azimuthal scan average is used.

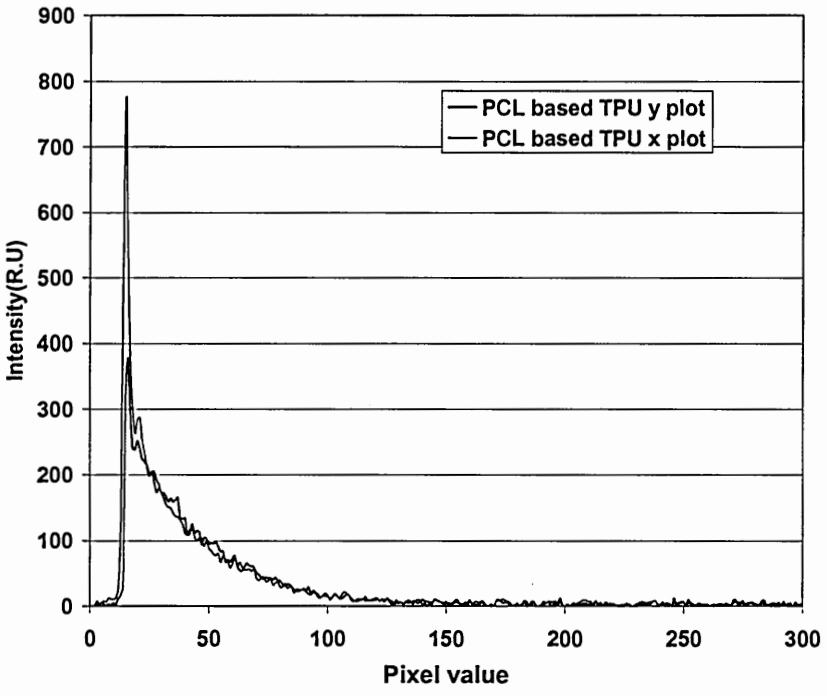

Figure 10. Comparison of meridian and equatorial intensity of the x-ray scattering of the PCL TPU filaments at 2 mm from die for data from BNL synchrotron SAXS

The approach taken for data handling and correction was to first convert from pixel position to scattering angle and scattering vector k. Silver behenate standard was used for this conversion. An estimated coefficient of absorbance was calculated by fitting the tail of the background scattering (I vs K) and sample scattering to a linear equation. A true coefficient of absorbance could not be calculated for this analysis because it was logistically impossible to measure background intensity directly after every single exposure to the x-ray beam since the fiber extrusion process was dynamic. Stopping the extrusion process and starting up again in between each sample spinning would have created extreme time delays during the experiment. This experiment is relatively unique given its dynamic nature. The traditional methods to correct data could not be followed. The following relationship describes how the data were corrected for background scattering:

I(k)= sample intensity – (air intensity * coefficient of absorbance)

The data were averaged azimuthally to obtain the final curve for analysis.

Two approaches were used to analyze the data generated at BNL; the Guinier, and the Debye approach.[16, 22] The Guinier approach is used for systems with a single particle size and shape and a low concentration of scatterers. Equation 14 for dilute systems can be rearranged with the following format:

$$\ln[I(k)]_{k \to o} = -\frac{k^2 R_g^{\ 2}}{3} \tag{23}$$

At very small scattering angle, a plot of the log intensity as a function of the square of the scattering angle, k^2, would yield a straight line with a slope equal to $-\frac{1}{3}R_g^{\ 2}$ where R_g is the radius of gyration. This plot is known as the Guinier plot.

The Debye approach was discussed on page 16. The Debye approach requires a plot of $\frac{1}{\sqrt{I(k)}}$ vs. k^2 yield a straight line.

Normalization of the relative invariant The PCL TPU compression-molded films and the PTMO TPU solution-cast films were considered equilibrated structures because the phase segregation process was optimized. The relative invariant from the two equilibrated structures was normalized to give a value of 100. All other samples were then normalized with respect to the equilibrated structures. To compare the BNL

data with the other data a 48 hour aged material was measured at BNL and in Roswell. While this is not an absolute determination of the invariant, this approach allowed the comparison of level of phase segregation in relative terms. Data from seconds old filament from the BNL data to days old from the K-C data, both synchrotron and standard SAXS can be compared by this method.

Dynamic Mechanical Analysis

Theory When a cyclic load is applied to any elastomer, not all of the input energy is recovered when the sample is relaxed. Some of the input mechanical energy is converted into heat and the other portion is used for recovery. The portion of the energy that is lost is known as hysteresis. DMA measures the ability of a viscoelastic material to store and dissipate mechanical energy. [23] DMA measurements are based on the differences in the load response of the viscous and elastic components to a small sinusoidally applied strain. The strain in this study was applied by cycling the sample in a tension-tension mode. The resulting stress is measured using an appropriate sensor. Figure 11 illustrates, schematically, the theory behind a typical DMA experiment. The resultant stress lags behind the applied strain by a phase angle δ, which is also shown in the figure. For a perfectly elastic material, which stores all the input energy, the phase lag will be 0° and for a perfectly fluid (viscous) material it will be 90° out of phase. Thus the stress and strain are in phase for an elastic material.

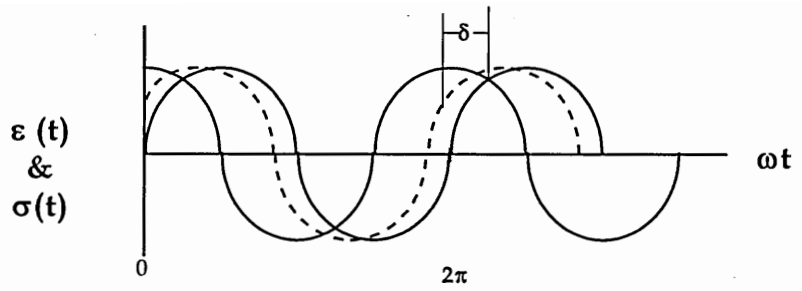

Figure 11. The imposed strain (sine wave), stress response (cosine wave, completely viscous) and intermediary stress response (viscoelastic material out of phase with the applied strain by a phase angle δ).

In DMA experiments frequency can be varied at a constant temperature and vice-versa. (In this study a single frequency was used with various temperatures). Generally, in constant frequency experiments, a low frequency such as 1 Hz is chosen since secondary transitions and other structural features can be easily detected. In addition, results of low frequency measurements can also be related to data obtained from other techniques. It is well known that time (frequency) and temperature have opposite effects on molecular motion.

Dynamic results obtained in tension-tension mode may be expressed in terms of the complex modulus, E*, the ratio of the tensile stress to tensile strain. Figure 12 gives a schematic representation of how the complex modulus or compliance can be resolved into its components. Equation 24 gives the resolution of the complex modulus and a similar equation for compliance can also be written. The E' component, in phase, gives a measure of the energy stored and recovered in each strain cycle. It also gives a measure of the stiffness or strength of a material. The loss modulus E" gives a measure of the energy dissipated or lost as heat per cycle for a given strain amplitude.

$$E^* = E' + i\,E'' \qquad (24)$$

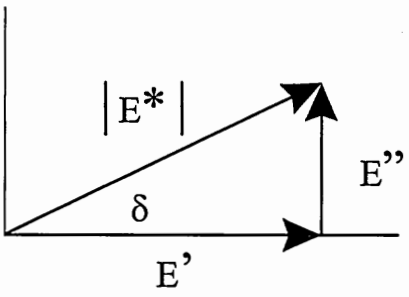

Figure 12. Vectorial resolution of the complex modulus

Tan δ is the ratio of the loss to stored modulus and is a measure of the ratio of the energy lost to energy stored in a cyclic strain loop. Equation (25) gives a mathematical representation of tan δ. Tan δ must be "zero" for a perfectly elastic material and "infinity" for a completely inelastic material.

$$\tan \delta = E''/E' \qquad (25)$$

Measurements Dynamic mechanical measurements were performed on a Rheometrics scientific DMTA V at a constant frequency of 2 Hz. The testing was made on filaments oriented along the extrusion direction in the tension – tension mode using sinusoidal stress oscillations. The temperature sweep varied from –125°C to 200°C during the test. Each approximately 1 mm diameter filament specimen was analyzed for approximately one hour to produce storage modulus (E'), loss modulus (E''), and loss tangent (tan δ) profiles.

Differential Scanning Calorimetry

The thermal response curves from samples were obtained using differential scanning calorimetry (DSC) using a TA Instruments MDSC 2920, V2.5A. The samples were equilibrated at -125°C for 10 minutes and subsequently heated at a rate of 10°C / minute to 250°C. Samples were cut to a weight range between 5-15 milligrams. Data were collected at 2.5 points per second. Transition temperatures were derived from the inflection points on heat flow verses temperature curves for each material. All testing was performed in an N_2 gas atmosphere.

Tensile Testing

Tensile testing was performed on single filaments of the samples. The filament was clamped between the jaws of a MTS Sintech 1/S testing frame, set at a 2" grip-to-grip distance. The displacement of the crosshead was set to a speed of 20"/minute. The filaments were stretched to break at room temperature. Using the calculated cross-sectional area and initial distance between the grips, the engineering stress and percent elongation were calculated. The modulus of elasticity was obtained by applying rubber elasticity theory.[1] The value of Young's Modulus (E) is calculated by taking the initial slope of the stress extension rate at very small extension rates (Stress vs elongation $(\alpha - \frac{1}{\alpha^2})$) and estimating that slope as shear modulus (G). The elastic modulus (E) can be calculated using the equation E = 2(1+v)*G for rubbery materials with a Poisson ratio of 0.5; E is 3xG.

Hysteresis

The hysteresis data at room temperature was obtained using a MTS Sintech 1/S frame. The filaments were clamped between the jaws of the Sintech at a 3" grip-to-grip distance. The filaments were stretched to 100% elongation with the crosshead moving at a speed of 20 inches/ minute and returned to the starting point. This procedure was repeated for three cycles. The area under the loading and unloading curves was calculated to obtain the energy loss according to Equation 26:

$$\%\text{Hysteresis} = \frac{(\text{Loading energy} - \text{Unloading energy}) * 100}{\text{Loading Energy}} \tag{26}$$

The hysteresis and set values were obtained for an upper elongation limit of 200% for the filaments. Set is the difference in distance between the onset of zero load at the beginning and end of a cyclic deformation.

RESULTS AND DISCUSSION

Small Angle X-Ray Data Analysis

Analysis of the PTMO and PCL TPU Equilibrium Structures In order to compare morphologies of the TPU polymers of this study with the non-equilibrium structures created in commercial production setups, it was necessary to estimate the equilibrium morphology. Two approaches were used to develop samples that have the highest level of phase separation possible with these two TPU polymers. The first approach was to produce a solution-cast film slow-cooled and left to evaporate slowly in an oven under vacuum. The second approach was to create a slow-cooled compression-molded film and then allow it to cool to room temperature over night. These samples may not provide the ideal equilibrium structures, but provide a level of phase segregation sufficient to analyze the data generated in this study of the two TPU systems being considered. Samples are compared to these practical equilibrium structures.

Figure 14 shows the corrected intensity versus the scattering vector, k, for the equilibrated structure of the solution-cast PTMO TPU film. The Debye method, which considers the total intensity of the scattering curve, was used to analyze these data. Figure 15 shows the 1/sqrt I versus k^2 Debye plot.

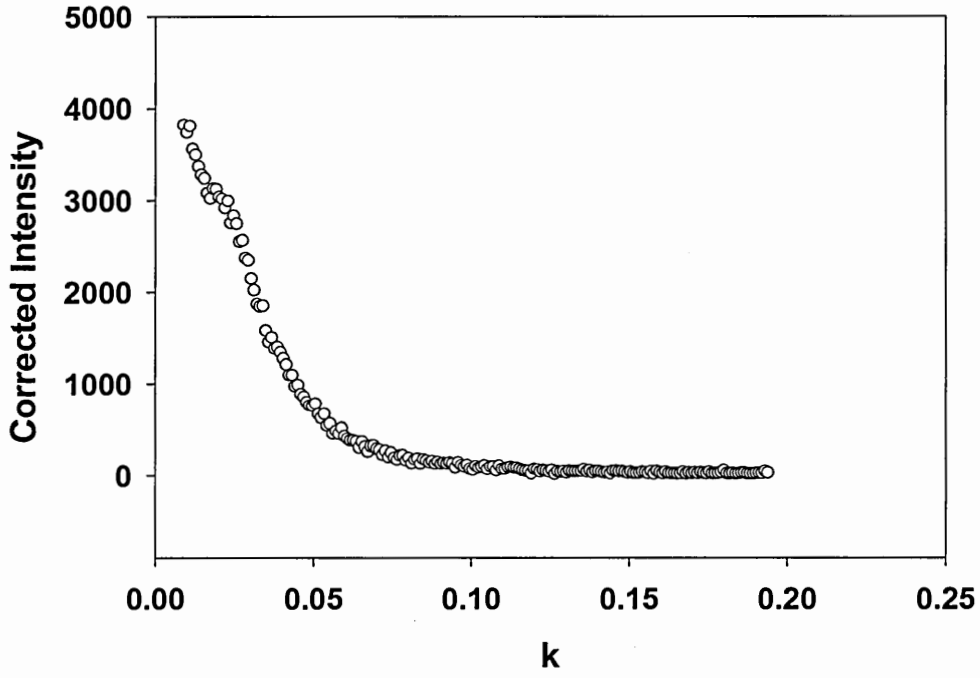

Figure 14. SAXS plot of the solution-cast film of the PTMO TPU

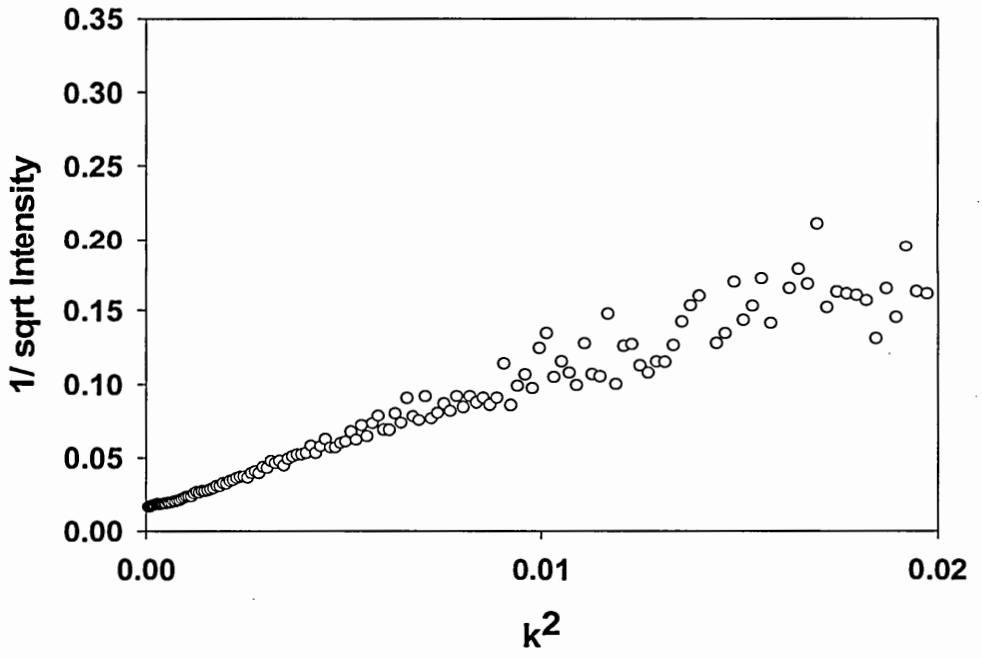

Figure 15. Debye plot for the solution-cast film of PTMO TPU

The Debye correlation length for the solution-cast film calculated using Equation 18 was found to be approximately 24 Å. Using Equation 20, the hard domain size of the solution-cast PTMO TPU film was estimated to be 100 Å. The domain morphology of the same Dow PTMO TPU was studied with tapping mode AFM by McLean and Sauer (1997).[24] The results of the study indicate that small hard segment domains are randomly dispersed in a continuous soft phase. The hard domains are described by McLean as heterogeneous and polydisperse in comparison to the more regular and well defined structure of a styrenic block copolymer. The TPU systems examined in the current study are expected to have very similar irregular domain morphology.

The Debye procedure could not be used for the solution-cast PCL TPU since WAXS analysis of the solution-cast film showed a crystalline peak that was not present in the extruded filament structure as seen in Figure 16. Examination of the equilibrium DSC thermogram shown in Figure 51 indicates the existence of a crystalline peak. The position and temperature of melting of the peak suggests that the peak is associated with the hard domain. In order to make a meaningful comparison between the film and the filament, the SAXS data were obtained on a melt-compressed slow-cooled film sample. Figure 17 shows the completely amorphous WAXS curve of the compression molded film of PCL TPU. Figure 18 shows the plot of intensity versus scattering vector for this sample. It can be seen from this figure that there is a peak present in the scattering intensity plot centered at $k = 0.035$ Å^{-1}. The presence of the peak suggests the existence of hard domain in the PCL TPU. The Debye approach could not be used to analyze these data. The Debye approach assumes random order and size, an assumption not consistent with the data. Instead, the one-dimensional correlation function developed by Vonk (Equation 16) was used to analyze the data. The 1-D correlation function is plotted as a function of the distance in real space (x).

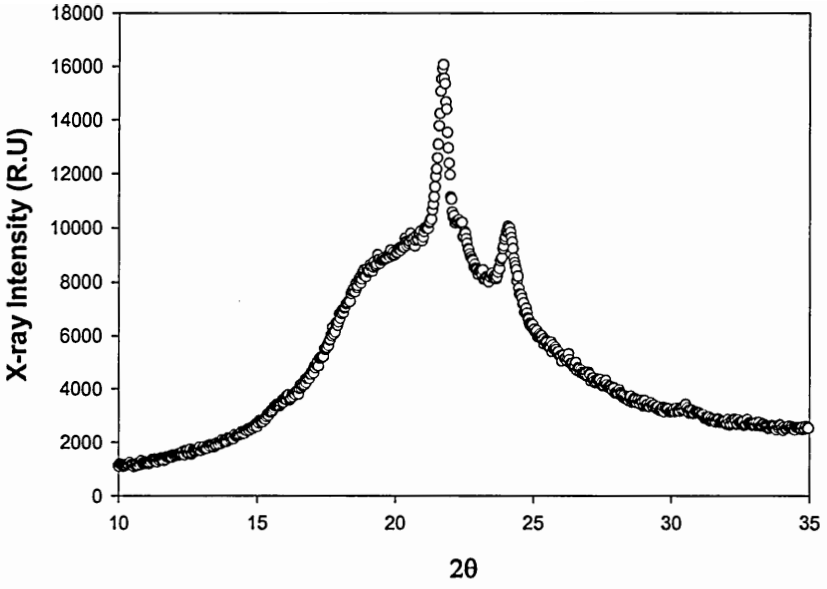

Figure 16. WAXS curve of the PCL TPU solution cast film showing crystalline structures

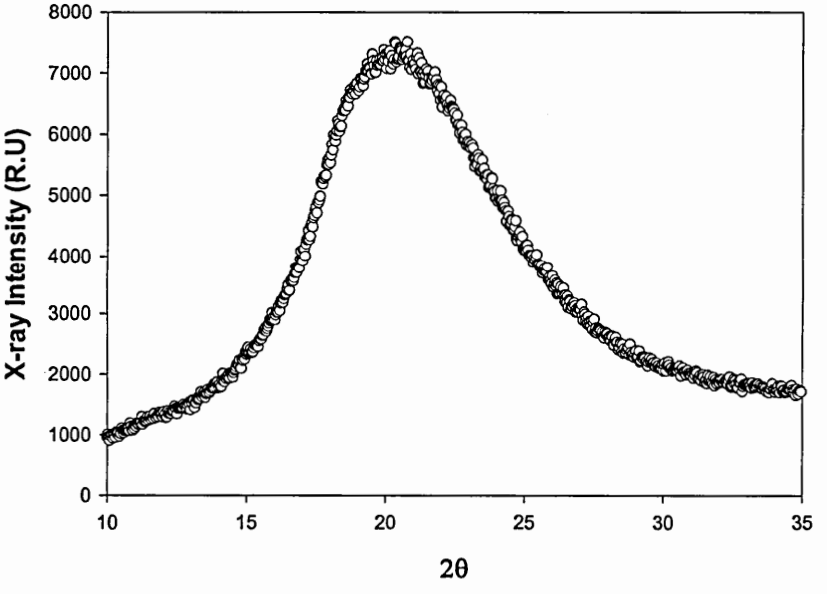

Figure 17. WAXS curve of the PCL TPU compression molded film showing completely amorphous structure

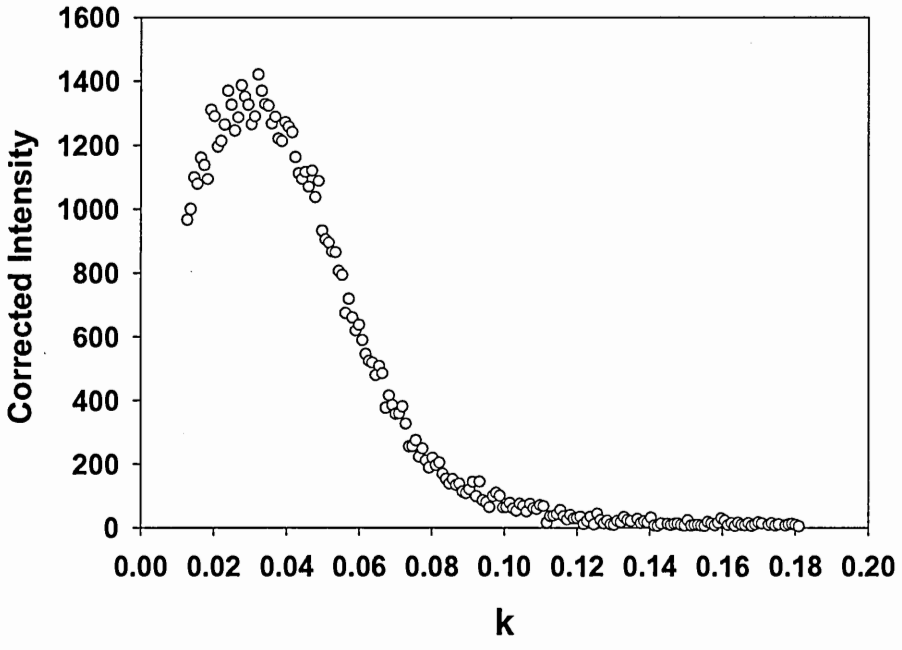

Figure 18. The scattering curve of the slow cooled compression-molded film of PCL TPU

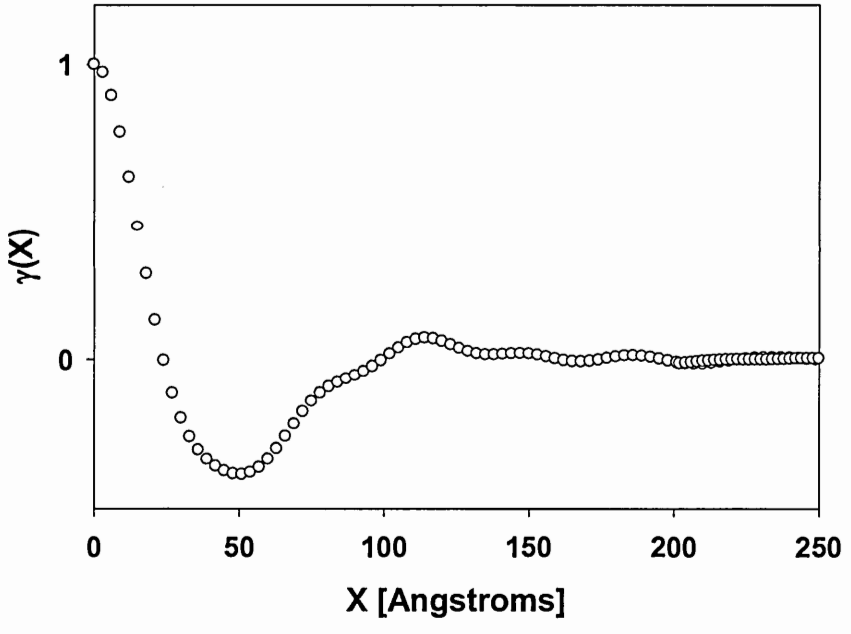

Figure 19. Vonk 1-D correlation function plot for the slow-cooled compression-molded film of PCL TPU

The average interdomain spacing obtained from the location of the first maximum of the plot shown in Figure19 is 114 Å for the equilibrium structure of the PCL TPU. It can be seen from this figure that the first maximum is not very well defined. This indicates that the morphology of the PCL TPU slow-cooled compression-molded film is not a true lamellar structure but is something between a lamellar aggregation and a random type of morphology. The order in the system is only consistent through small distances. There is definitely no long-range order in this polymer since no second-order peaks appear in this system. Previous studies of TPU polymers have shown similar shapes of the scattering curve.[8]

SAXS analysis of in-situ spun TPU at BNL Figures 20a, 20b and 21a, 21b show the corrected scattering curves for the PTMO and PCL TPUs exposed to the synchrotron beam. It can be seen from these Figures that the intensity decreases smoothly from small to large angles. In general, TPU polymers phase separate relatively slowly compared to other elastic block copolymers like styrenic block copolymers.[4] The shapes of these curves suggest partially phase-mixed systems. The lack of higher order diffraction patterns in the scattering curve also support this hypothesis.

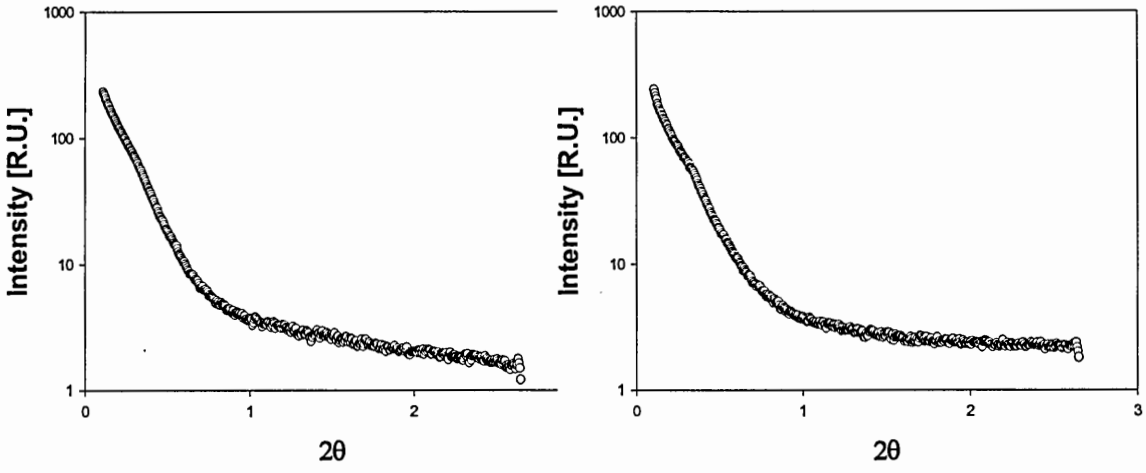

(a) (b)

Figure 20. Corrected SAXS intensity versus scattering angle for TPU filaments from BNL synchrotron experiment (a - PCL TPU at 2 mm from die, and b - PCL TPU at 24 mm distance from the die).

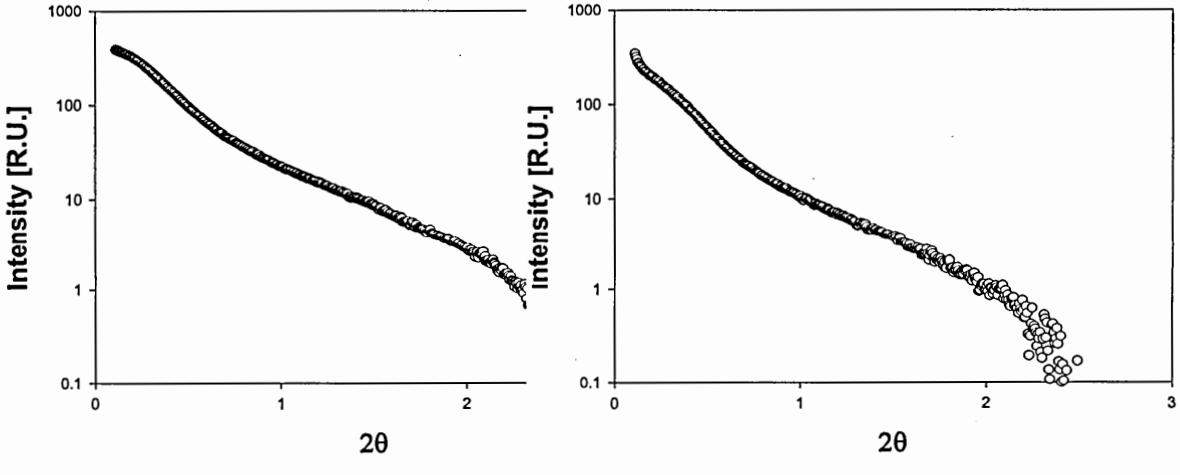

(a) (b)

Figure 21. Corrected SAXS intensity versus scattering angle for the TPU filaments fro BNL synchrotron experiment (a - PTMO TPU at 2 mm from die, and b - PTMO TPU at 24 mm distance from the die.

Hence, two approaches were used to analyze the data—the Guinier for single particle and the Debye approach for scattering of particles of different sizes and shapes. Figure 22 shows the Guinier plot for the PCL TPU polymer. The shape of the curve deviates from a straight line behavior; therefore the Guinier method assumptions are not valid. Nevertheless, a fit of the curve to a straight line was executed and a slope of the curve was extracted resulting in an approximate estimation of domain size. From this curve, the domain size for the PCL TPU was estimated to be 40 Å (slope=-510, R^2= 0.98).

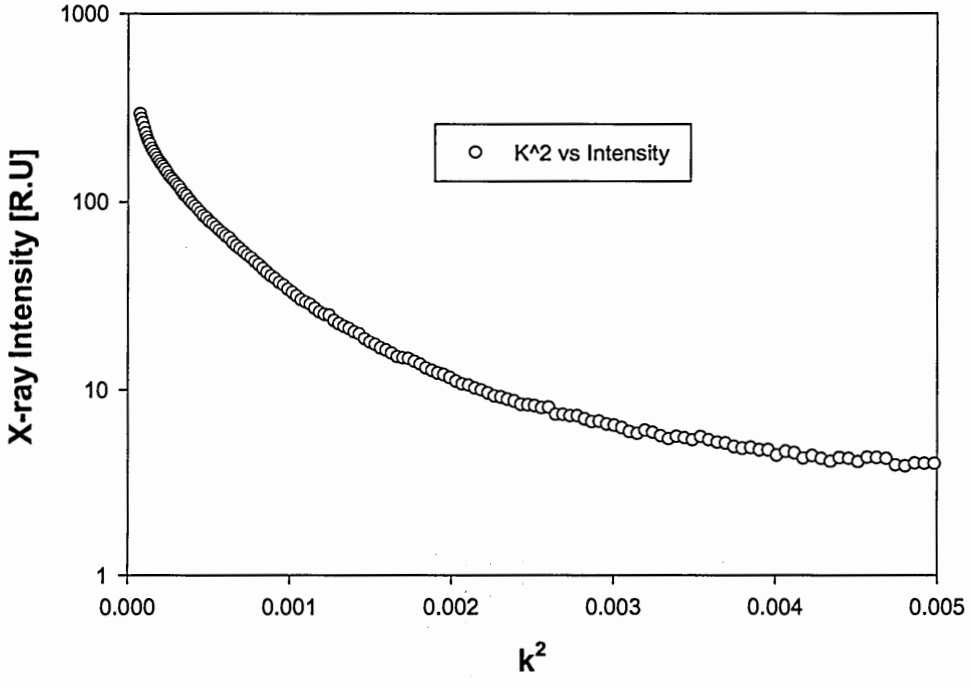

Figure 22. Guinier plot of the scattering of the PCL TPU 24 mm from the die from BNL

The lack of a linear fit of the data to the Guinier approximation prompted the analysis of the data by the Debye approach. The Debye method was used to analyze these data to see if the random model better describes the scattering curve.

Figure 23 shows a Debye plot of $\frac{1}{\sqrt{I}}$ vs. k^2 for the PCL TPU according to equation 19. This figure confirms that the Debye model describes the systems better than the Guinier model. Then again, it is not surprising that the systems are described by the Debye model if one considers the way the samples were made at high shear and cooling rates. The fact that the filaments measured at BNL for both TPUs and the compression-molded films of the PCL TPU made at K-C are better described by the Debye approach implies that these systems have non-uniform distribution of domains.

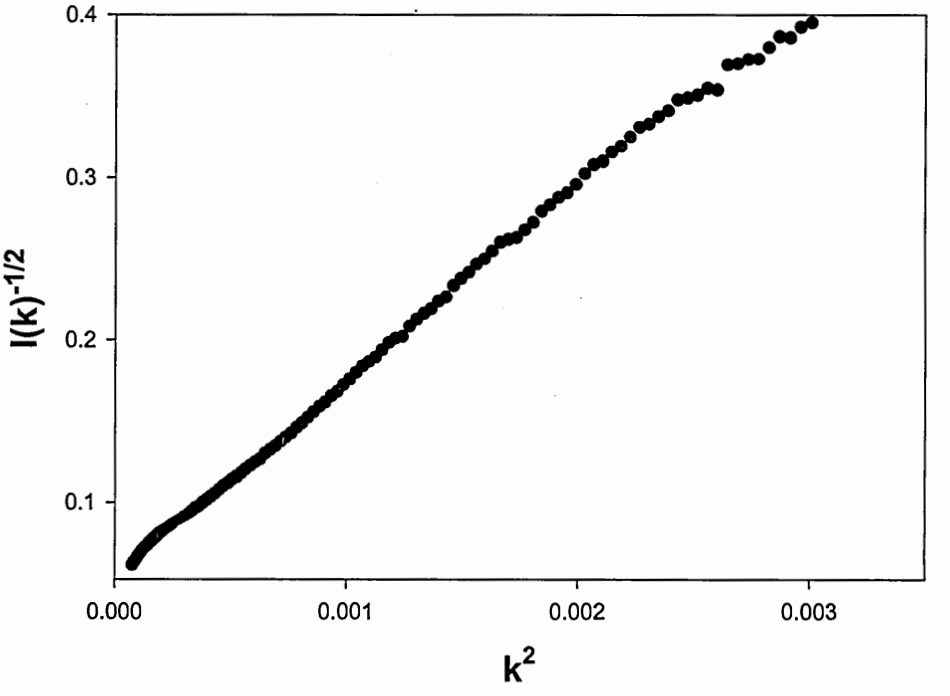

Figure 23. Debye plot of PCL TPU measured at 24 mm from the die at BNL

The analysis of this plot gives a correlation distance (distance between hard domains) of a=43 Å ($a= (110/0.06)^{1/2}$, $R^2= 0.99$).

Figures 24 and 25 show the I vs 2θ curves for the in-situ spun PTMO and PCL TPU polymer at BNL. These plots indicate that the intensity as a function of distance from the spinneret increases. Both PTMO and PCL TPUs show a peak at very low 2θ values. The filaments were also measured at 48 hours from extrusion time at BNL; this data is also present in Figures 24 and 25.

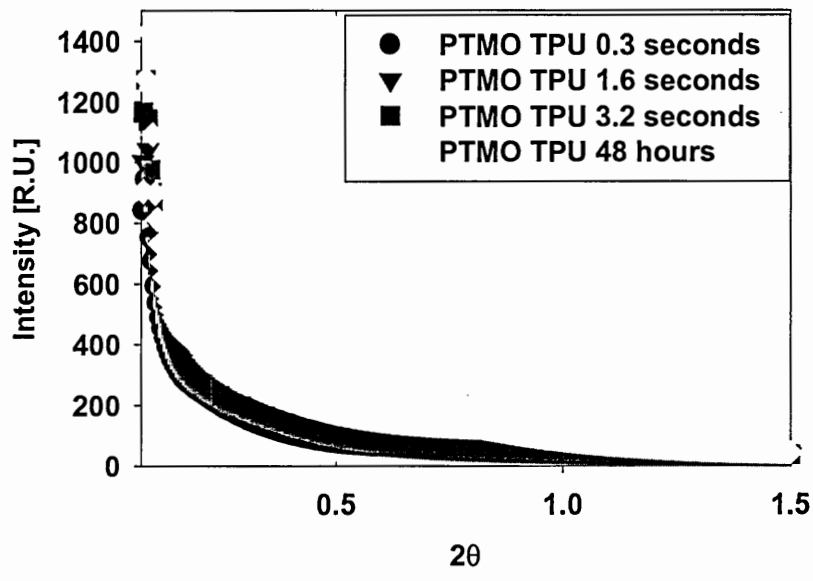

Figure 24. Plot of I vs. 2θ for the PTMO TPU measured at BNL at positions from 2 to 24 mm from the extruder die. The filaments were also measured 48 hours after they were extruded at BNL.

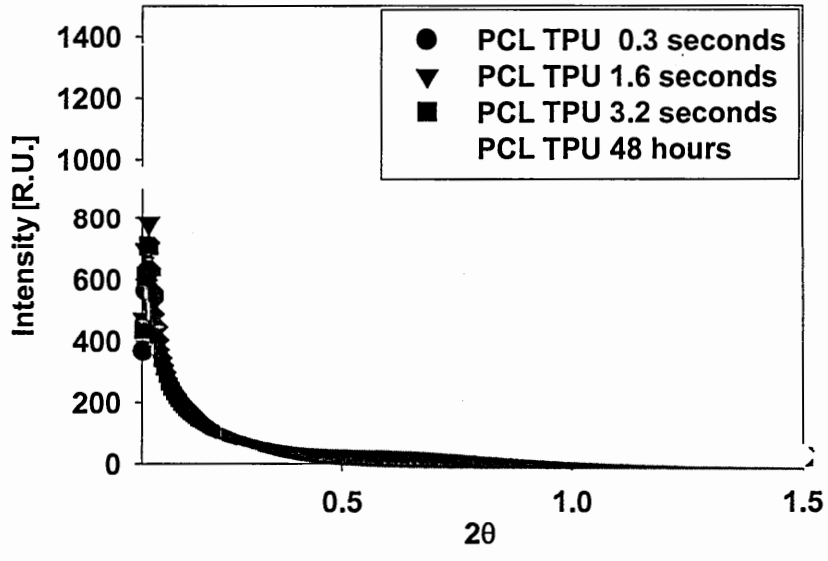

Figure 25. Plot of I vs 2θ for the PCL TPU measured at BNL at positions from 2 to 24 mm from the extruder die. The filaments were also measured 48 hours after they were extruded at BNL.

Table 4 shows the domain size as a function of time analyzed according to the Debye approach. The table also shows the relative invariant calculated according to Equation 23.

Table 4. SAXS data calculations from BNL data- Debye correlation length, hard domain size and relative invariant

TPU, SS	Time (s)/Distance (mm)	Debye length Å	Hard Domain size Å	Relative Invariant, Q $(e/vol)^2$
PTMO	0.3/2	16 ±0.8	58	28
PTMO	1.6/12	17±0.8	62	31
PTMO	3.2/24	22±1.1	78	31
PTMO	48 Hours	24±1.2	86	60
PCL	0.3/2	42±2.1	107	21
PCL	1.6/12	33±1.7	83	25
PCL	3.2/24	41±2.1	103	24
PCL	48 hours	30±1.5	75	92

Note: The time from the die was calculated by estimating the velocity of the filament based on the pump rate, capillary exit diameter, and polymer density and finally the distance measurement was taken from the die exit. Using this method the data can be compared later to the longer time analysis.

Table 4 shows that for the PTMO TPU, the domain size increases as a function of distance/time. This implies that the phase segregation is occurring as a function of time for this polymer. Examination of the PCL TPU shows that the data do not show a similar trend with time and distance. The PCL TPU exhibits better thermodynamic compatibility between the soft and hard phases than the PTMO TPU which appears to limit the phase segregation seen with the PCL TPU system. Solubility parameters were calculated for the two TPUs using the group contribution method.[23] The resulting

solubility parameter for the MDI hard segment extended with the butane diol is a value of 17 $J^{\frac{1}{2}}/cm^{\frac{3}{2}}$. The PCL soft segment has a calculated solubility parameter of 16 $J^{\frac{1}{2}}/cm^{\frac{3}{2}}$ and the PTMO solubility parameter was calculated as 12 $J^{\frac{1}{2}}/cm^{\frac{3}{2}}$. The PTMO and MDI hard segment have a greater difference in solubility parameter value and so have a higher thermodynamic drive to phase segregate compared to the MDI and PCL combination.

On average, the domain size of the PCL TPU is larger than the PTMO TPU. This observation is not unexpected since the PCL TPU has 39% compared to the 24 wt % hard segment content of PTMO TPU. The higher percent hard segment in combination with the higher compatibility of the hard domains with the soft phase also would contribute to the size of the domain. The domains will be larger and ill-defined for the PCL TPU.

Figure 26 shows a comparison of the Debye plots for the PCL TPU and PTMO TPU filaments at distances corresponding to 0.3 and 3.2 seconds after exiting the die.

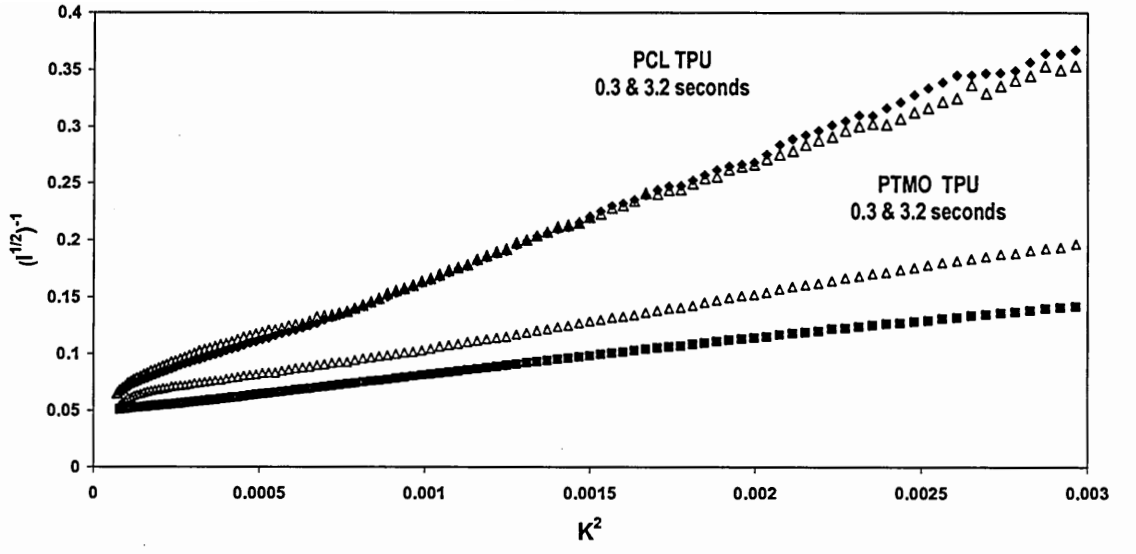

Figure 26. Debye plots for the PTMO and PCL TPUs from BNL SAXS data

Analysis of Figure 26 shows that the PTMO TPU develops an increase in slope with time when comparing the lines at 0.3 and 3.2 seconds. The PCL TPU also shows a change in slope with time but this is much smaller in magnitude than the slope change with the PTMO TPU.

Analysis of SAXS data across time

Kinetics of phase segregation -PTMO TPU Two sets of experiments were completed for the examination of domain morphology. The first set of experiments was done at BNL with the synchrotron x-ray source studying morphology within the first few seconds of extrusion. The second set of experiments was done at K-C on a single screw extruder with either a chilled or room temperature roll. The domain morphology of the filaments generated at K-C was studied between 15 minutes after extrusion to weeks after extrusion. Tables 5 and 6 give the results of the SAXS analysis done on the PTMO

TPU by the Debye methods. The SAXS data was collected on filaments extruded at Kimberly-Clark Corporation using a Brabender extruder and collected on a casting roll chilled to 60°F or at room temperature 72°F (RT). The data in Table 5 begins at 0.25 hours because there was no way to logistically cast a filament specifically onto a chilled roll and test it before that time. The filaments made at BNL were measured within the first few seconds after extrusion. The filaments extruded at K-C are measured in a longer time frame of minutes to hours and days from extrusion and so are referred to as longer time experiments.

On average the accuracy of the Debye plot line fit gave a 90% confidence level for the Debye correlation length calculation. The statistical relevance of the relative invariant was considered by calculating the number of points assessed in the relative invariant. This number is very large for the SAXS data. For instance, the solution cast PTMO TPU film experiment there were 312 pixels and the total corrected intensity was 142,441 units. The product of this gives a value of N=44,441,598 units which then can be related to the statistical relevance of the data through the relationship of $1/\sqrt{N}$. The large N value used for the invariant analysis lead to a very small statistical variability.

Table 5. PTMO TPU Chill Roll SAXS data for longer time experiments

Time (Hr)	Debye length (Å)	Relative Invariant
0.25	14±0.7	83
1	16±0.8	85
3	16±0.8	88
24	17±0.8	91
72	18±0.9	94
192	17±0.8	94
312	18±0.9	99
336	18±0.9	96
600	18±0.9	96
Solution Cast	20±1	100

Table 6 shows the data collected on filaments extruded onto a room temperature roll at BNL (0.001 to 48 hours) as well as the longer time data collected at Kimberly-Clark (1 hour to 10000 hours). The BNL and K-C extrusion systems are different. The BNL filament extrusion system is a small melt index plunger apparatus, whereas the K-C filament extrusion system is a single screw extruder. These two systems differ in many aspects including shear rate and dwell time. Interestingly, when comparing the data taken at 48 hours at BNL and the 24 and 72 hour data taken at K-C, there is a good correlation in domain size and relative invariant value between the two extrusion systems.

Table 6. PTMO TPU- BNL and KC extruded onto a roll @ RT data

Time (Hr)	Debye length (A)	Relative Invariant
0.0001	16±0.8	28
0.0004	17±0.9	31
0.0009	22±1.1	31
48	24±1.2	60
1	15±0.8	45
24	24±1.2	58
72	24±1.2	63
168	22±1.1	92
Solution Cast	24±1.2	100

Figure 27 shows a plot of the data presented in Tables 5 and 6. The data of the equilibrium structure obtained at 10,000 hours is not included in this figure. This figure indicates that the domain size of samples collected on a chilled roll is smaller than that of samples collected on the room temperature roll. This could be because the room temperature roll is warm enough to allow mobility of the polymer segments which then associate and form larger domains.

Analysis of the relative invariants of the both the BNL and K-C generated PTMO TPU filaments illustrates that the samples which were chilled tend to have higher overall phase segregation. The magnitude of the relative invariant is higher for the chilled roll samples compared to the samples which were collected on a room temperature roll. It takes almost 168 hours before the room temperature roll sample reaches the same level

of segregation as the solution-cast film based on comparison of the relative invariant values. It seems that the chilled roll fixes the size of the domains at an early stage of phase segregation but the number of hard domains is larger for the chilled roll cast filaments than the filaments cast onto a room temperature roll.

The results of this study suggest that the chilling of the PTMO TPU during processing will allow the formation of better defined domains. Smaller sized, well segregated domains are expected to impart better elastic and mechanical properties to the polymer. The analysis of the thermal and mechanical properties may shed some light into this hypothesis.

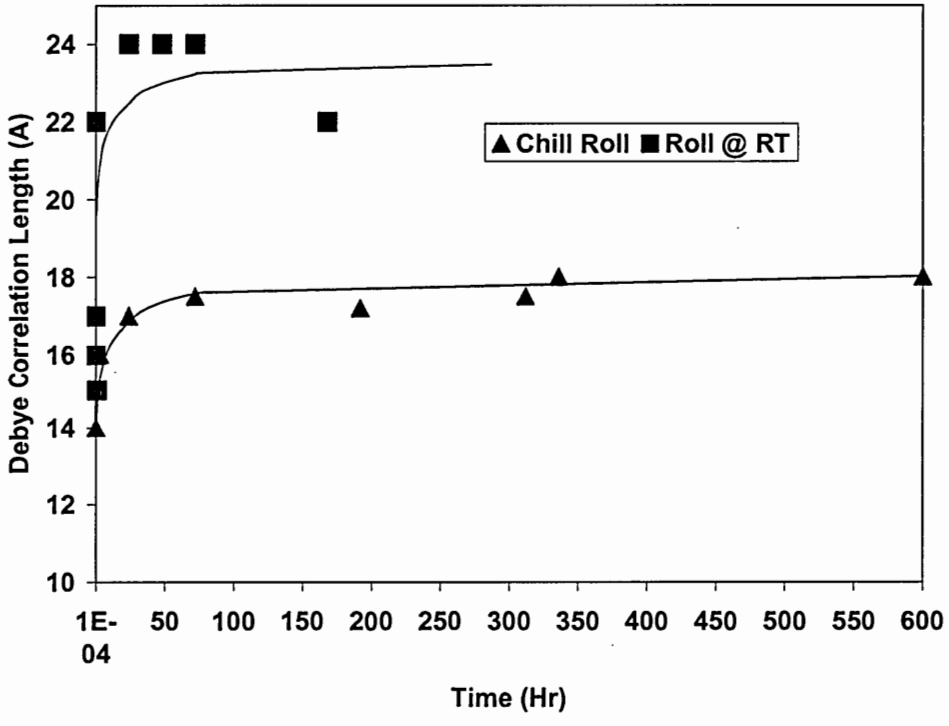

Figure 27. Chart of the Debye correlation length as a function of time for the PTMO TPU filaments collected on both chilled (extruded at K-C) and room temperature rolls (extruded at both BNL and K-C) .

Examination of the relative invariant data plotted in Figure 28 suggests that the PTMO TPU can follow two different pathways as it approaches the equilibrium state of segregation. The relative invariant for the filaments extruded onto a chilled roll is larger across time. The relative invariant for the filaments extruded onto a room temperature roll is lower immediately after extrusion and then increases with time but does not reach the value of the chilled filaments until days after extrusion. Filaments collected on the roll at room temperature remain phase mixed indicated by a smaller relative invariant, while extruding to the chilled roll appears to provide a desired phase segregated structure. This implies that the analysis of the kinetics of phase segregation has to be completed separately for the chilled roll and room temperature roll cases.

The arguments presented above can be illustrated by plotting the log of relative invariant as a function of log time. Figure 28 shows that the filaments collected on the chilled roll and the room temperature roll follow two different kinetics of phase segregation. The filaments collected on the room temperature roll segregate at a faster rate than the filament collected on the chilled roll. These results are consistent with expectations.

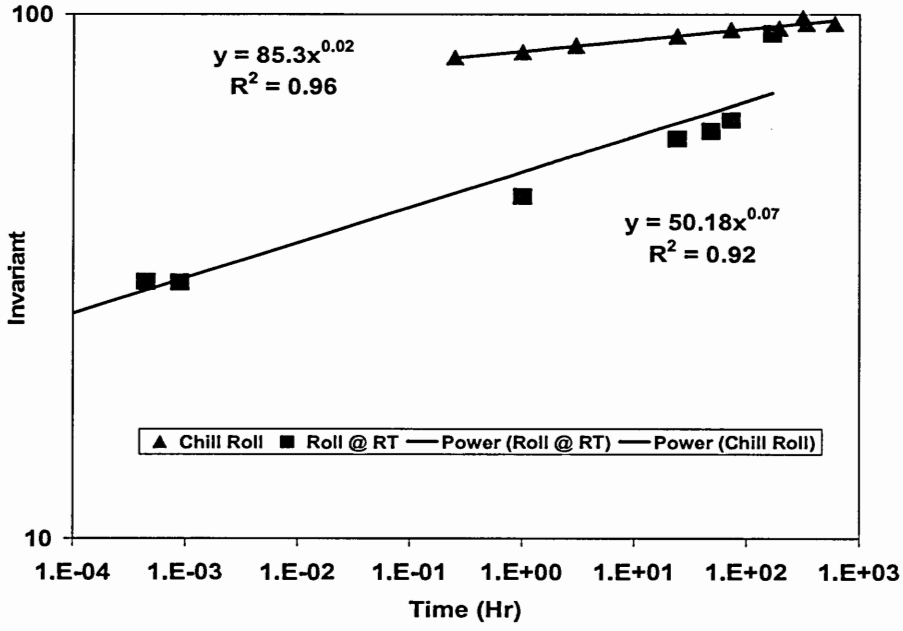

Figure 28. Plot of the relative invariant as a function of time for the chilled roll and room temperature roll PTMO TPU samples

In order to see if the Debye correlation length and the relative invariant are consistent with a similar mechanism of phase segregation, all data was combined and analyzed. The graphical representation of these data is below in Figure 29. The plot shows a very poor correlation of the Debye length as a function of time which may mean that Debye assumptions are not valid throughout the duration of the evolution of the domain structure. Both the Debye and the Vonk modeling approaches should be employed to analyze full range of phase segregation across time.

A combined treatment of the relative invariant across all time shows a better correlation than analyzing the data by the Debye correlation length alone. The slope of the overall curve follows a pattern closer to the one that was seen with the room-temperature roll alone. It follows that the kinetics of phase segregation are greatly influenced by the annealing conditions. Hence, a comparison of the magnitude of the

regression coefficients for the filaments extruded under different conditions indicates that the samples collected on a chilled roll and room-temperature roll follow two different rates of phase segregation.

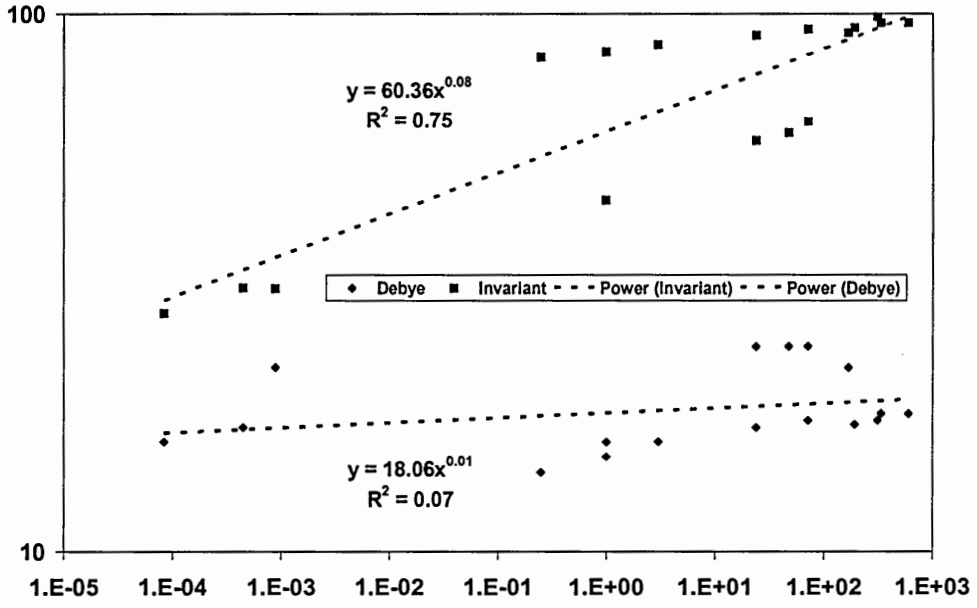

Figure 29. Comparison of the Debye correlation length and the relative invariant for the PTMO TPU extruded onto the room temperature roll

Both Tables 5 and 6 also contain two additional samples which were solution cast, and compression-molded for the PTMO and PCL TPUs respectively. These samples were made for use as optimized phase segregated structures. The reason for making these samples was to compare them with the in-situ and delayed time spun filaments already described to get a measure of how close to an ideal structure the extruded filaments could get with time and differing process conditions.

Kinetics of Phase segregation - PCL TPU

Tables 7, 8, and 9 show the characteristic parameters obtained for the PCL TPU by SAXS analysis. Table 8 also includes the results of data obtained from BNL. The 48 hour SAXS data shown in Table 8 was obtained on the same BNL spun filament sample after waiting two days.

Table 7. Debye analysis of PCL TPU filaments extruded onto a chilled roll at K-C

Time (Hr)	Interdomain spacing (A)	Invariant
0.25	88±9	80
1	89±9	83
3	88±9	87
24	87±9	92
72	88±9	92
192	90±9	97
336	88±9	98
600	90±9	97
compression molded	115±12	100

Table 8. Debye analysis of PCL TPU filaments extruded onto a room temperature roll at BNL

Time (Hr)	Debye length (Å)	Invariant
0.0001	42±2.1	21
0.0004	33±1.7	25
0.0009	41±2.1	24
48.00	30±1.5	92

Table 9. Vonk analysis of PCL TPU filaments extruded onto a room temperature roll at K-C

Time (Hr)	Interdomain spacing (Å)	Invariant
1	80±8	66
3	82±8	77
24	80±8	92
72	80±8	93
168	81±8	93
compression molded	115±12	100

Figure 30 shows the interdomain d-spacing calculated for the PCL TPU filaments extruded at K-C. Figure 30 also shows the Debye correlation length calculated using the synchrotron generated data from filaments extruded at BNL. Examination of Figure 30 shows a big scatter in the Debye correlation length. At very short duration of exposure (synchrotron beam), the domains are not segregated enough to apply the Vonk method to analyze the data. However, the data collected on one of these filaments after 48 hours shows a Debye correlation length that is too low. This would imply that in 48

hours the equilibrium morphology has been developed and the Debye approach to reduce the data is no longer valid. Under these circumstances the data should be analyzed by Vonk's method. Examination of the magnitude of the relative invariant given in these tables also suggests that this conclusion is appropriate. All domain d-spacings calculated for the longer time experiments attain a plateau quickly. The chilled roll samples give a higher d-spacing than samples collected on the room temperature roll. This observation indicates that the domains are smaller and closer for the filaments spun on to the room temperature roll. The magnitude of the relative invariant attains an equilibrium value of ~92 $(e/vol)^2$ in about 24 hours as also can be seen from these tables.

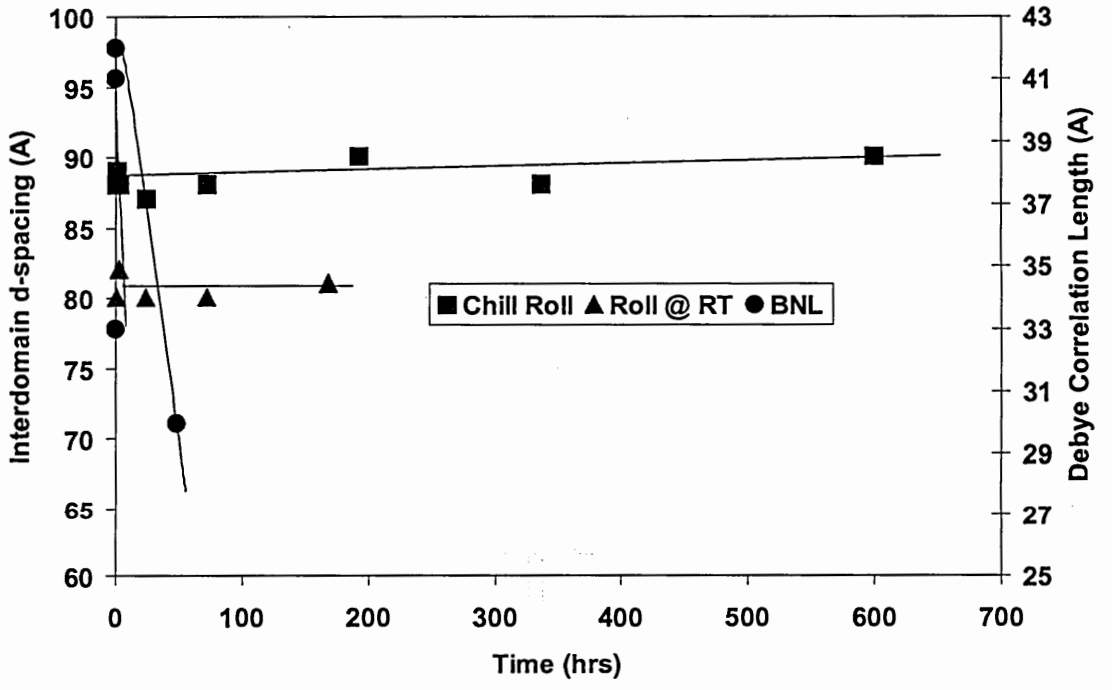

Figure 30. Interdomain d-spacing (green and red) and Debye correlation length (blue) as a function of time for the PCL TPU filaments spun under various conditions

The interdomain d-spacing of the PCL TPU provided in Table 9, however, does not change with time. The spacing is approximately 80 Å and stays the same as a function of time. The relative invariant shows a systematic change up to 24 hours. Again, it appears that the purification of the hard domains by the rejection of soft blocks or the creation of new domains would account for this observed effect.

As in the case of the PTMO TPU samples, a better approach to understand the phase segregation process is to analyze the relative invariant. Figure 31 shows a plot of the relative invariant as a function of time for the PCL TPU filaments extruded at BNL and Kimberly-Clark. This figure illustrates that the phase separation is a slow process and suggests the synchrotron beam is able to capture the evolution of the domain as a function time. In all cases the relative invariant attains a constant value in about 24 hours. Figure 31 shows the plot of the relative invariant as a function of time for the BNL, chilled roll, and room temperature roll filaments. Examination of the slopes of the curve shown in Figure 31 indicate that the phase segregation at short time (BNL) takes place faster than for the filaments collected on a room temperature roll, which in turn, is faster than the filaments collected on a chilled roll.

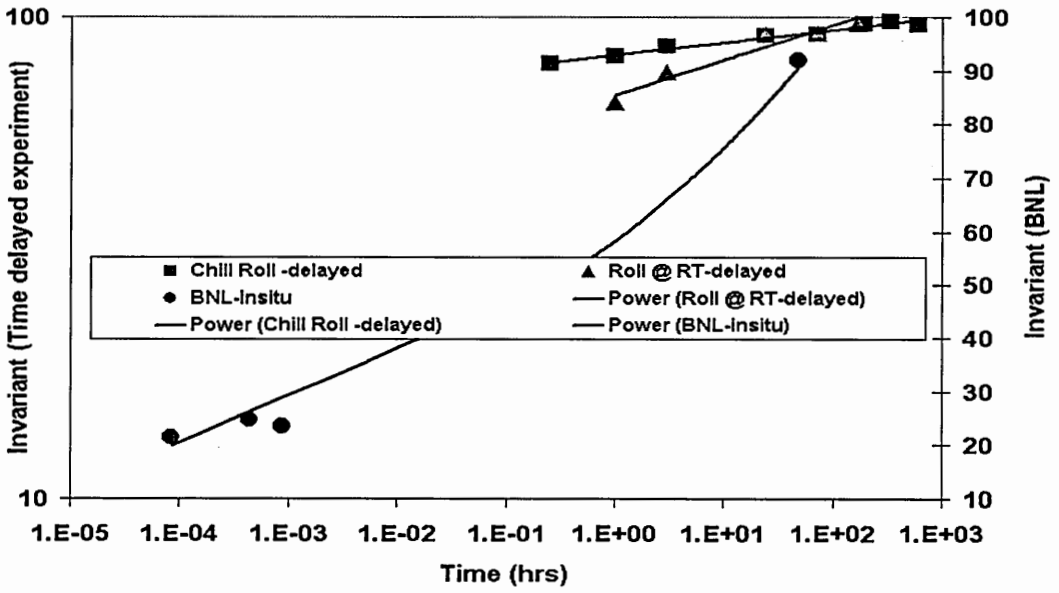

Figure 31. Combined plot of the relative invariant for all PCL TPU data from chill roll and room temperature extruded filaments as a function of time. The trend lines of the data are $y = 9x^{0.072}$ $R^2 = 0.94$ $y = 58x^{0.11}$ $R^2 = 0.98$ $y = 83x^{0.03}$ $R^2 = 0.97$ for the chilled roll data, the room temperature roll data and the BNL data respectively.

Figure 32 is a plot of all of the relative invariants for all filaments generated with PCL TPU as a function of time. Figure 32 combines the data obtained at BNL with the data from the chilled and room temperature rolls from K-C. Overlaying of all the data indicates that, irrespective of how the samples were made, they all tend to follow a similar trend. The PCL TPU is less sensitive to the conditions of extrusion than the PTMO TPU.

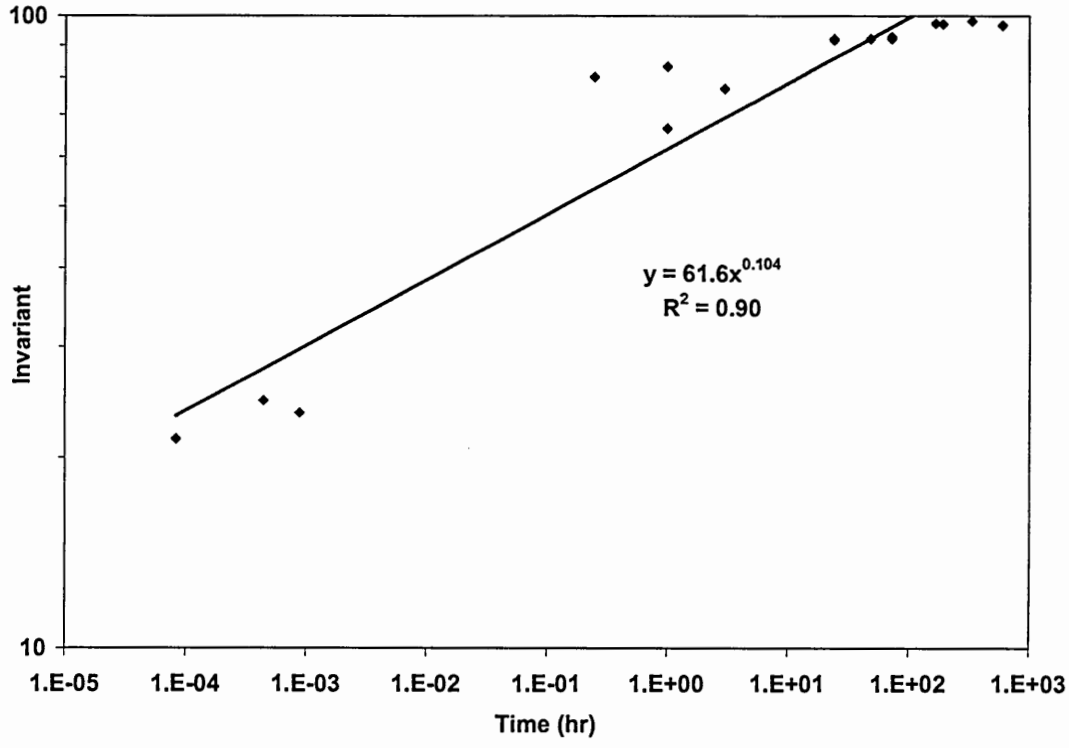

Figure 32. Plot of the relative invariant as a function of time for the PCL TPU spun at BNL, and the filaments generated in experiments (chilled and room temperature rolls) conducted at Kimberly-Clark Corp.

Mechanical Properties

DMA Figure 33 shows the normalized storage modulus as a function of temperature for the PTMO TPU extruded on the room temperature roll. The slope, or sharpness, of the down turn of the modulus vs temperature curve gives an indication of the level of the phase segregation of the soft segment. Higher slopes indicate better phase segregation. The plot in Figure 33 does not show a consistent trend of increasing slope with time. There is no clear trend of increasing segregation as a function of time. This erratic behavior of the storage modulus could be due to the competing mechanisms of crystallization of the soft (PTMO) block with that of the phase segregation process of the hard domains. As the hard segments are leaving the soft phase the soft block is

crystallizing, making it kinetically challenging to phase segregate. Examination of the DSC thermogram of the PTMO TPU shown in Figure 51 gives a melting endotherm centered around 10°C. Hence, the scattering differences detected in SAXS do not translate to differences in DMA results.

The change in peak position, as well as the sharpness of the tan δ curves, could also be used to understand the phase segregation process. The magnitude of the tan δ can be correlated with the degree of phase segregation and elasticity at a given temperature since it is the ratio of the loss to storage modulus (E"/E'). Analysis of Figure 34 indicates that the DMA spectra of the freshly prepared sample shows a phase mixed behavior since the tan δ curve falls off quicker than the rest of the curves which show a sharper peak. The peak positions, however, do not shift to a lower temperature as one would expect from better segregated system. The variability in the production of the filaments and testing logistics could reduce the sensitivity of the analysis of these types of measurements. One of the reasons could be that the magnitude and extent of the segregation process occurring on a molecular scale is not large enough to be reflected in the bulk properties of the filaments.

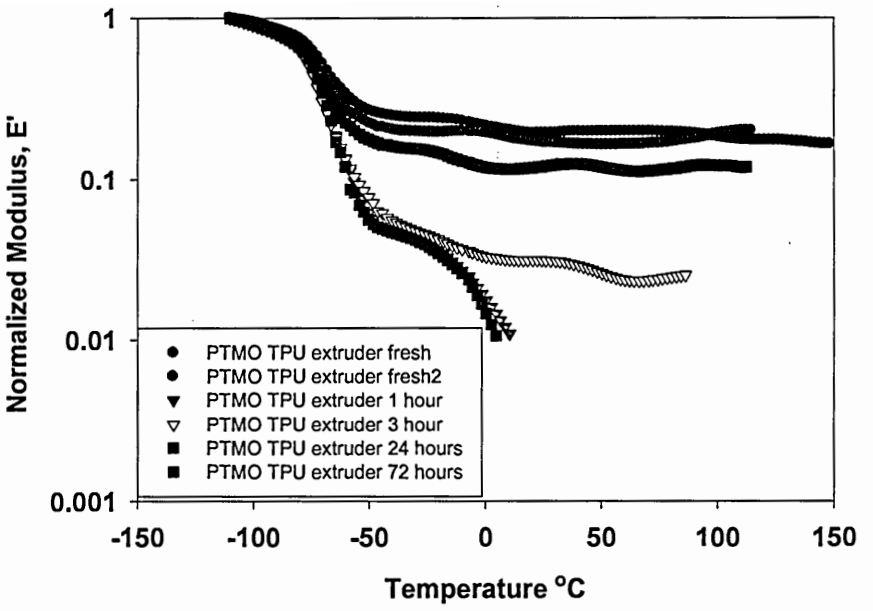

Figure 33. Normalized modulus as a function of temperature and time for the PTMO TPU collected on a room temperature roll

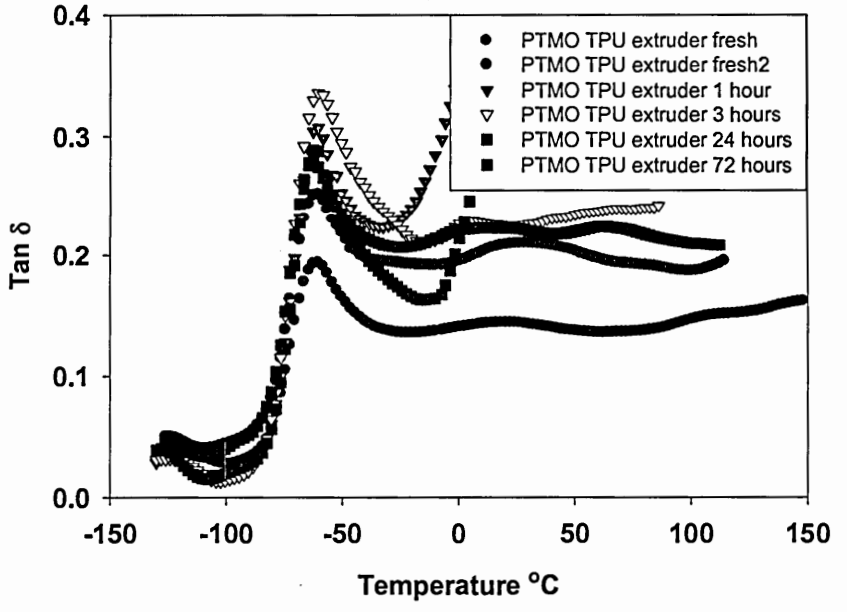

Figure 34. Loss tangent as a function of temperature and time for the PTMO TPU samples collected on a room temperature roll

Figures 35 and 36 show the normalized storage modulus and loss tangent as a function of temperature for the PTMO TPU collected on a chilled roll tested as a function of time. The three and eleven day samples show a trend where the rubbery modulus is lower than the rest of the samples. This indicates that the polymer has segregated reasonably well after three days.

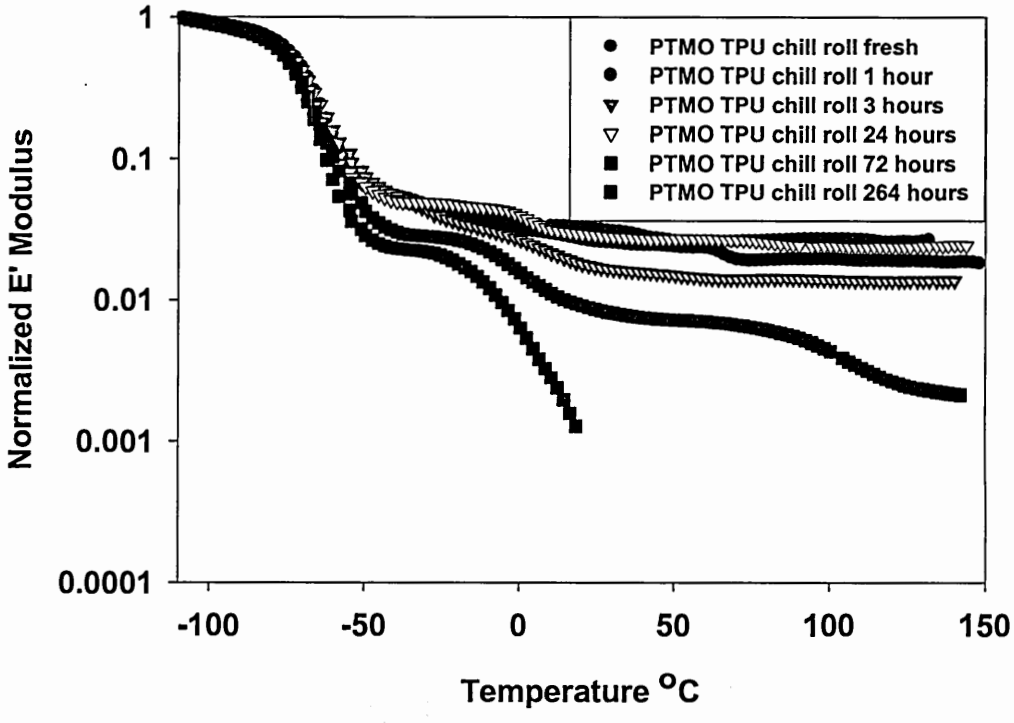

Figure 35. Normalized modulus as a function of temperature and time for the PTMO TPU collected on a chilled roll

The tan δ curves also become sharper with time indicating the continued purification of the soft domain as the system segregates. The behavior of the samples collected on the chilled roll is different from that of the room temperature roll. This closely follows the observation made with the relative invariant shown in Figure 28. The mechanism of domain formation might be different in these two cases. It should be

pointed out that the PTMO soft segment is capable of crystallizing at low temperatures and high elongations. The chilled roll samples show a trend that would be expected from a phase segregating system.

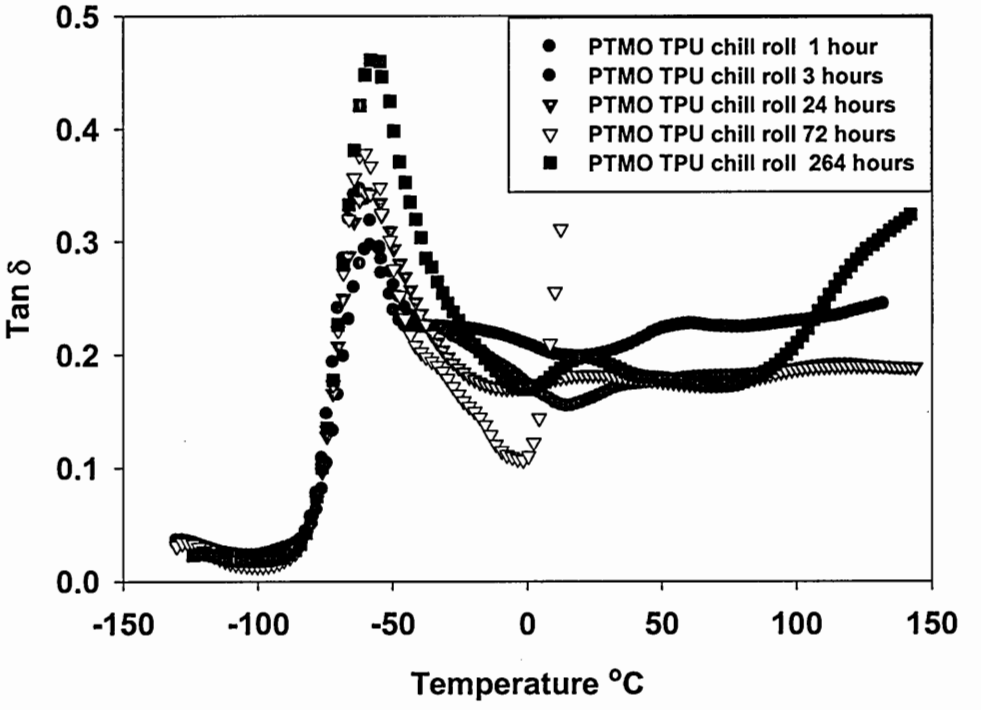

Figure 36. Loss tangent as a function of temperature and time for the PTMO TPU collected on a chilled roll

Figures 37 and 38 show the normalized storage modulus and tan δ for the PCL based TPU systems extruded onto a room temperature roll. These figures indicate that there are very negligible changes taking place in these samples as a function of time. This is in agreement with the interdomain d-spacing and relative invariant plots shown in Figures 30 and 31. The domain segregation, although not well defined, occurs so quickly it can only be seen in the BNL data; all other data show no change with time.

SAXS analysis also indicates that the formation of domains and growth is independent of the conditions under which the samples were collected and tested, i.e., chilled roll or the room temperature roll did not make any difference in this case. Hence, it is not surprising that the dynamic mechanical data of the PCL TPU presented in Figures 39 and 40 are very similar to the one shown in Figures 37 and 38 and therefore need no further discussions.

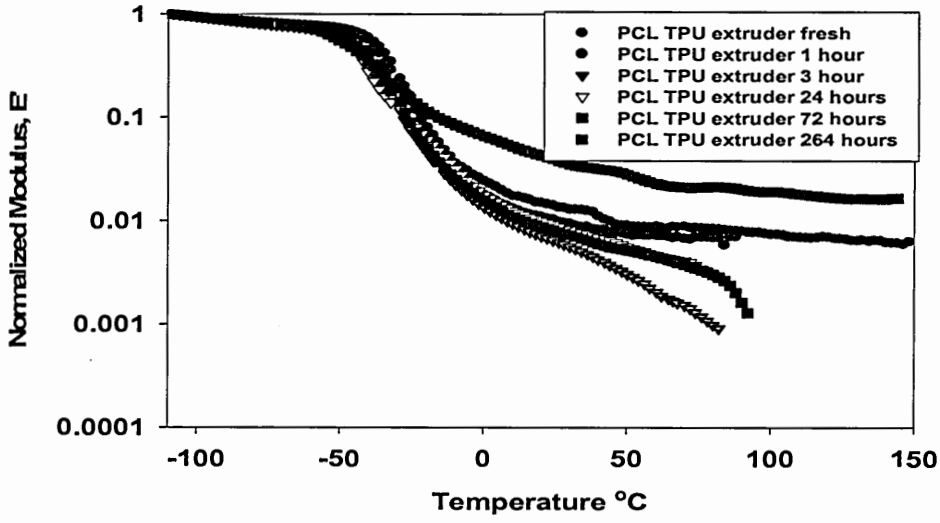

Figure 37. Normalized modulus as a function of temperature and time for the PCL TPU collected on a room temperature roll

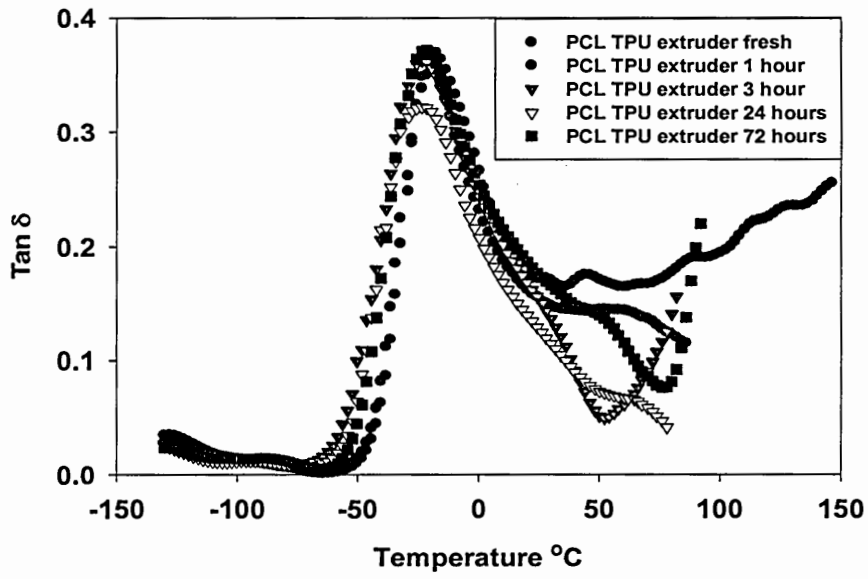

Figure 38. Loss tangent as a function of temperature and time for the PCL TPU collected on a room temperature roll

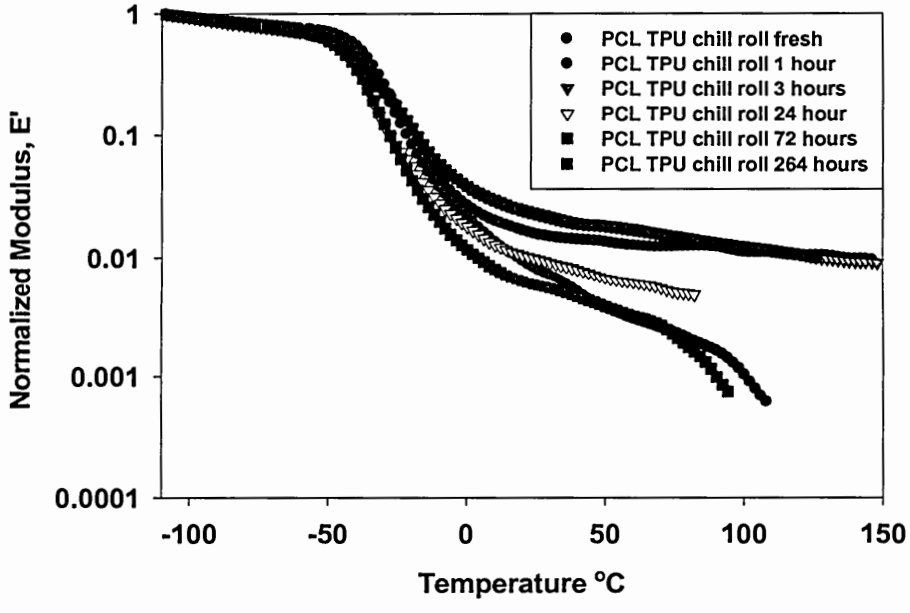

Figure 39. Normalized modulus as a function of temperature and time for the PCL TPU collected on a chilled roll

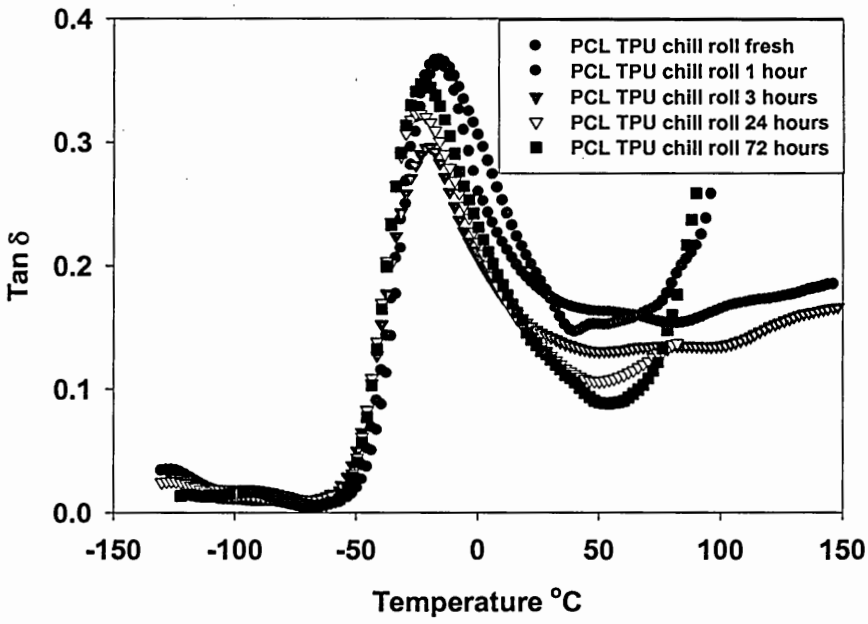

Figure 40. Loss tangent as a function of temperature and time for the PCL TPU collected on a chilled roll

The data shown in Table 10 indicates that the Tan δ maximum shows no trend of reduction of the tan δ maximum with aging time for the PTMO TPU. The table also shows no significant trend of reduction for the PCL TPU with aging time. This table does show that the two TPUs have different glass transition regions as indicated by tan δ maximum. The PTMO TPU has a much lower glass transition temperature than the PCL TPU. This indicates that the PTMO TPU is more mobile at the temperatures probed in this study. This increased mobility provided another advantage to the PTMO TPU for faster phase segregation kinetics compared to the PCL TPU.

Table 10. DMA Tan δ maximum for both the PTMO and PCL TPUs extruded at K-C as a function of time

Polymer Type	Casting roll	hours aged	Tan Delta peak temp °C
PTMO TPU	extruder	0	-60
PTMO TPU	extruder	1	-60
PTMO TPU	extruder	3	-60
PTMO TPU	extruder	24	-62
PTMO TPU	extruder	72	-62
PTMO TPU	extruder	264	-64
PTMO TPU	extruder	288	-62
PTMO TPU	chill roll	0	-58
PTMO TPU	chill roll	1	-61
PTMO TPU	chill roll	3	-58
PTMO TPU	chill roll	24	-60
PTMO TPU	chill roll	72	-62
PTMO TPU	chill roll	264	-58
PCL TPU	extruder	0	-18
PCL TPU	extruder	1	-19
PCL TPU	extruder	3	-21
PCL TPU	extruder	24	-24
PCL TPU	extruder	72	-22
PCL TPU	extruder	264	-28
PCL TPU	chill roll	0	-16
PCL TPU	chill roll	1	-16
PCL TPU	chill roll	3	-17
PCL TPU	chill roll	24	-22
PCL TPU	chill roll	72	-18
PCL TPU	chill roll	264	-18

Tensile Figures 41 and 42 show the stress-elongation behavior of some representative samples of the PTMO TPU collected both on the chill roll and the room temperature roll. These figures indicate that the materials show typical rubber elastic load-deformation behavior, i.e., the elongation of the order of 500% and greater. However, the filaments were not taken to failure since they were extremely tough and started slipping in the grips. As the polymer phase segregates the samples should show a decrease in modulus reflected by a decrease in initial slope. Figures 39 and 40 indicate that the tensile data did not correlate with the phase segregation process observed during the analysis of the SAXS data. One of the reasons could be that the magnitude and extent of the segregation process occurring on a molecular scale is not large enough to be reflected in the bulk properties of the filaments. Similar conclusions can be made about the PCL TPU. The stress elongation curves shown in figure 41 and 42 illustrate this point.

Several materials parameters (shear modulus, G, Young's Modulus, E, stress at yield, σ_y, elongation at yield, ε_y, stress at intercept, σ_i, elongation at intercept, ε_i) extracted from the stress-elongation measurements are shown in Table 11. It can be seen from the table that there is no increase or decrease in modulus as a function of time. Filaments cast on the chill and the room temperature rolls show the modulus as ±10 % which is within the statistical error of the method. Analysis of the data obtained for the PCL TPU samples also show a similar trend. However, as one would expect, the modulus of PCL TPU is much higher than the PTMO TPU. This is not surprising since the weight percentage of the hard segment in PCL TPU is much higher than that of the PTMO TPU. In addition, the PCL soft segment is much more compatible with the hard segment than the PTMO soft segment, both of which promote an increase in modulus.

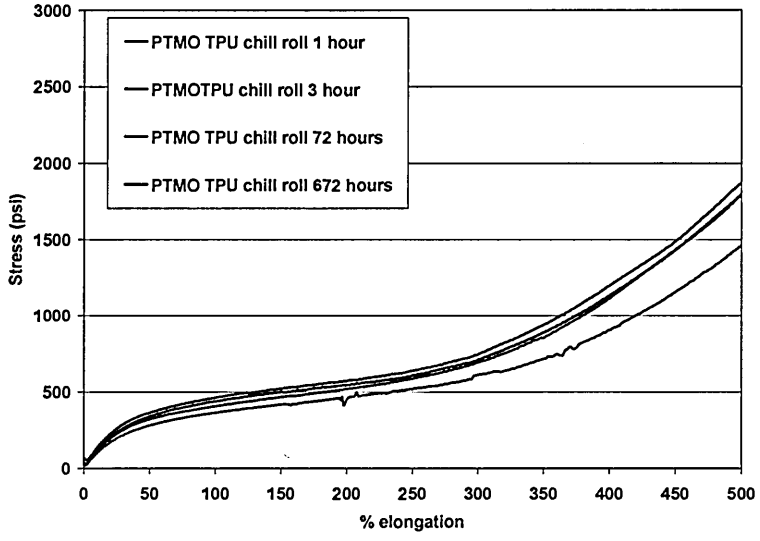

Figure 41. Stress-elongation curves as a function of time for the PTMO TPU collected on a chilled roll

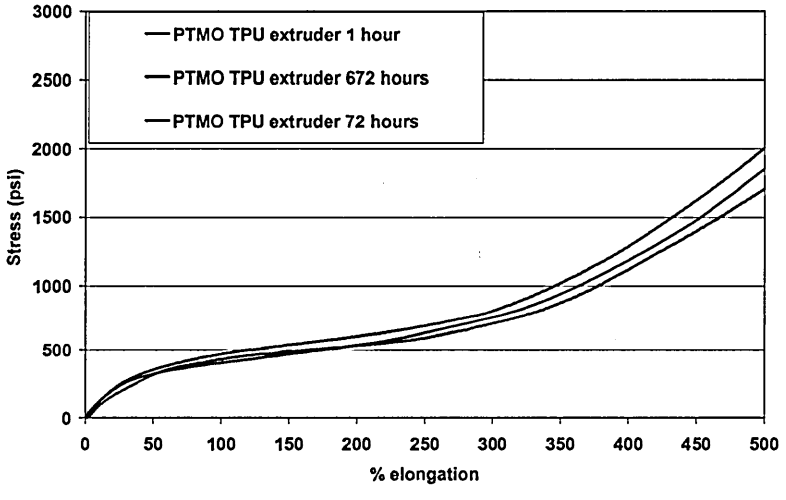

Figure 42. Stress-elongation curves as a function of time for PTMO TPU collected on a room temperature roll

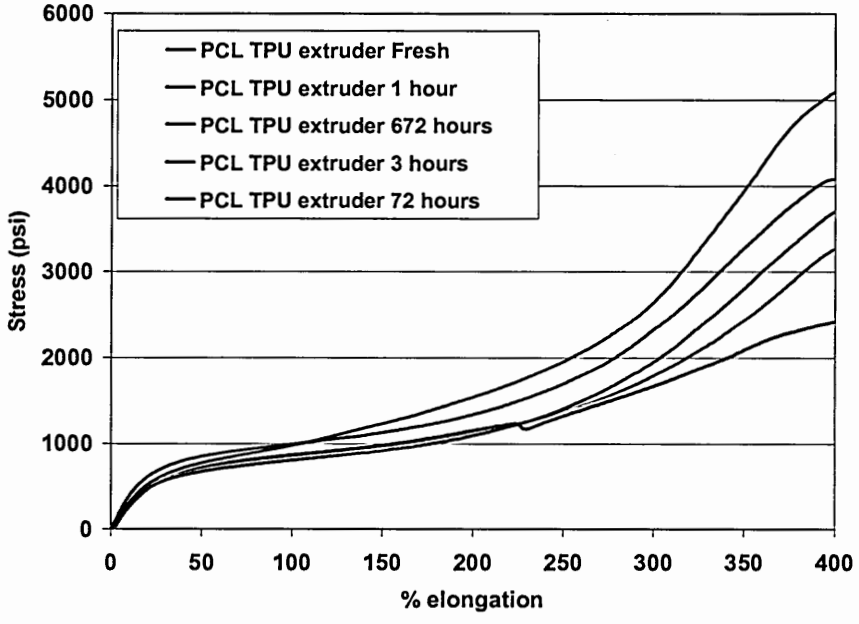

Figure 43. Stress-elongation curves as a function of time for the PCL TPU collected on a room temperature roll

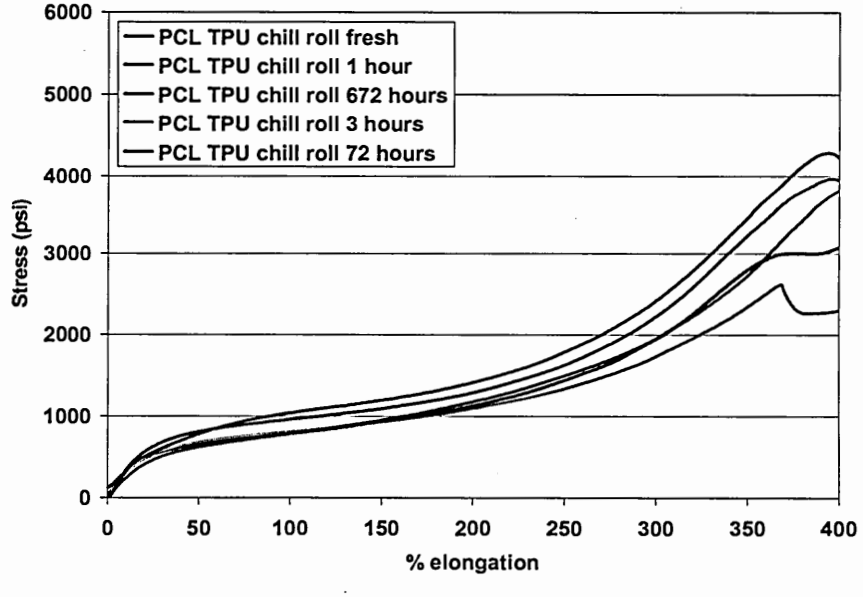

Figure 44. Stress-elongation curves as a function of time for PCL TPU collected on a chilled roll

Table 11. Summary of stress-elongation data for all codes

polymer	soft seg	position	age of sample	shear modulus G	modulus E	elong at yield %	stress at yield (psi)_	elong at intercept %	stress at intercept (psi)
2103-70a	PTMO	chill roll	fresh	600	1800	25	350	285	1075
2103-70a	PTMO	chill roll	1 hour	350	1050	33	290	420	720
2103-70a	PTMO	chill roll	72 hours	450	1360	27	380	370	810
2103-70a	PTMO	chill roll	7 days	380	1150	33	370	370	740
2103-70a	PTMO	chill roll	1 month	460	1380	35	390	368	780
2103-70a	PTMO	room temp	fresh	1200	3500	25	700	260	1800
2103-70a	PTMO	room temp	3 days	840	1800	30	440	400	900
2103-70a	PTMO	room temp	1 month	880	1140	55	400	320	880
2102-80a	PCL	chill roll	fresh	830	2500	28	550	290	1400
2102-80a	PCL	chill roll	3 hour	980	2900	25	630	290	1340
2102-80a	PCL	chill roll	24 hour	1100	3300	20	700	280	1400
2102-80a	PCL	chill roll	3 days	1340	4000	27	790	260	1370
2102-80a	PCL	chill roll	7 days	1283	3850	24	760	280	1470
2102-80a	PCL	chill roll	1 month	990	2970	25	800	280	1600
2102-80a	PCL	room temp	fresh	970	2900	23	670	270	1750
2102-80a	PCL	room temp	3 hour	960	2900	22	670	270	1790
2102-80a	PCL	room temp	3 days	1050	3150	23	600	280	1400
2102-80a	PCL	room temp	7 days	990	2970	20	540	280	1400
2102-80a	PCL	room temp	1 month	1340	4000	20	750	280	1480

Hysteresis Figure 45 shows the hysteresis behavior as a function of time using data obtained from a 200% cycle test for the PTMO TPU filaments collected on the chilled roll. Hysteresis results do not show a trend with increasing time. However, as shown in Table 12, the immediate set after the 2nd cycle decreases with time. This decrease is an indication of improved elastic properties over time via phase segregation. It appears that the changes in the sample set may provide a simple tool to follow the phase segregation process. More experiments have to be conducted to establish the validity of this approach. The same conclusions are valid for the PTMO TPU samples collected on the room temperature roll shown in Figure 46.

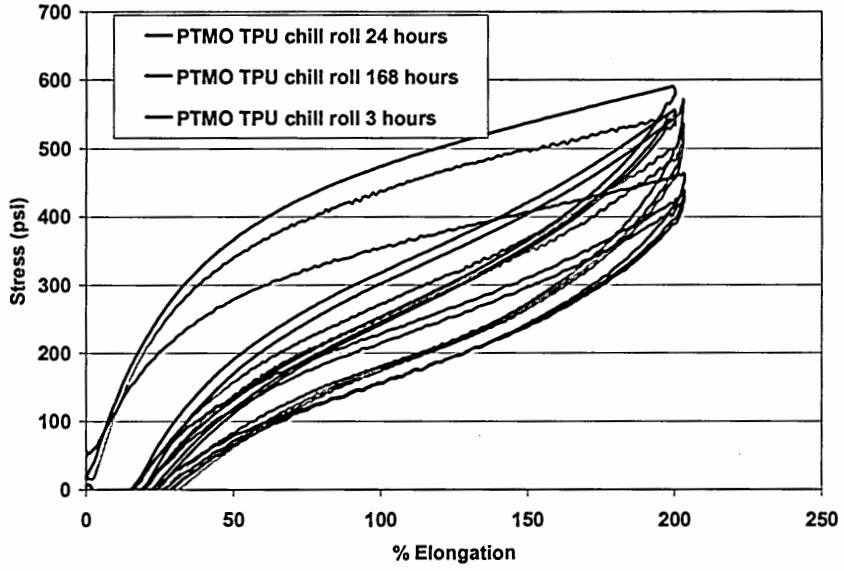

Figure 45. 200% elongation data three cycle hysteresis test curves for the PTMO TPU collected on the chilled roll and tested fresh, at 24 hours and 1 week of age

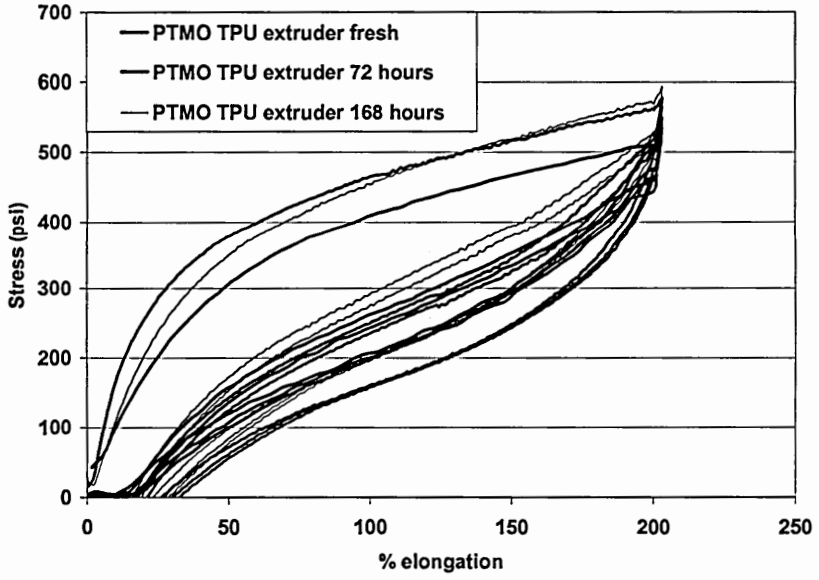

Figure 46. 200% elongation data three cycle hysteresis test curves for the PTMO TPU collected on the room temperature roll and tested fresh, at 72 hours and 1 week of age

The hysteresis data provided in Figure 47 for the PCL TPU chilled roll sample show a decrease of the stiffness as a function of time but no change in the hysteresis as seen in Table 12. Again, as in the previous case of the PTMO TPU, the set values decrease over time. This observation can be compared with the SAXS data shown in Table 7. Table 7 shows small but measurable increases of the relative invariant with aging. The results from both methods, SAXS and hysteresis set, indicate a finite improvement in phase segregation as a function of time.

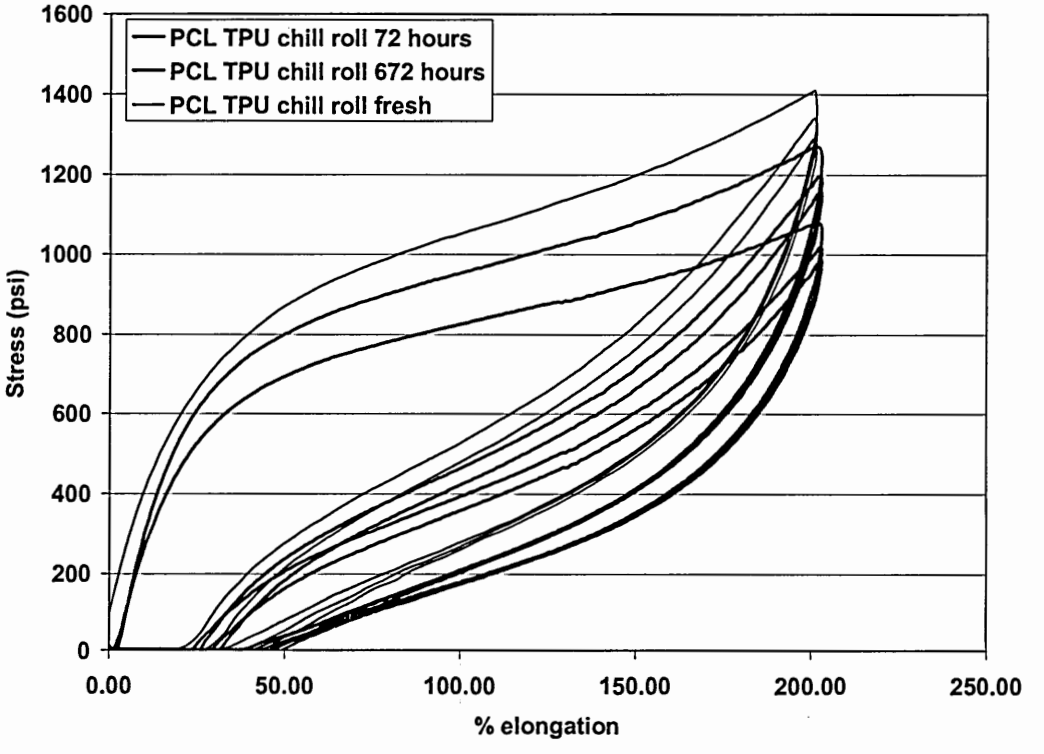

Figure 47. 200% elongation three-cycle hysteresis test curves for the PCL TPU collected on a chilled roll and tested fresh, at 72 hours and 1 week of age.

Figure 48 shows the hysteresis curves for the PCL TPU samples collected on a room temperature roll. The hysteresis data indicate no trend as a function of time but, the set data does show an improvement with time.

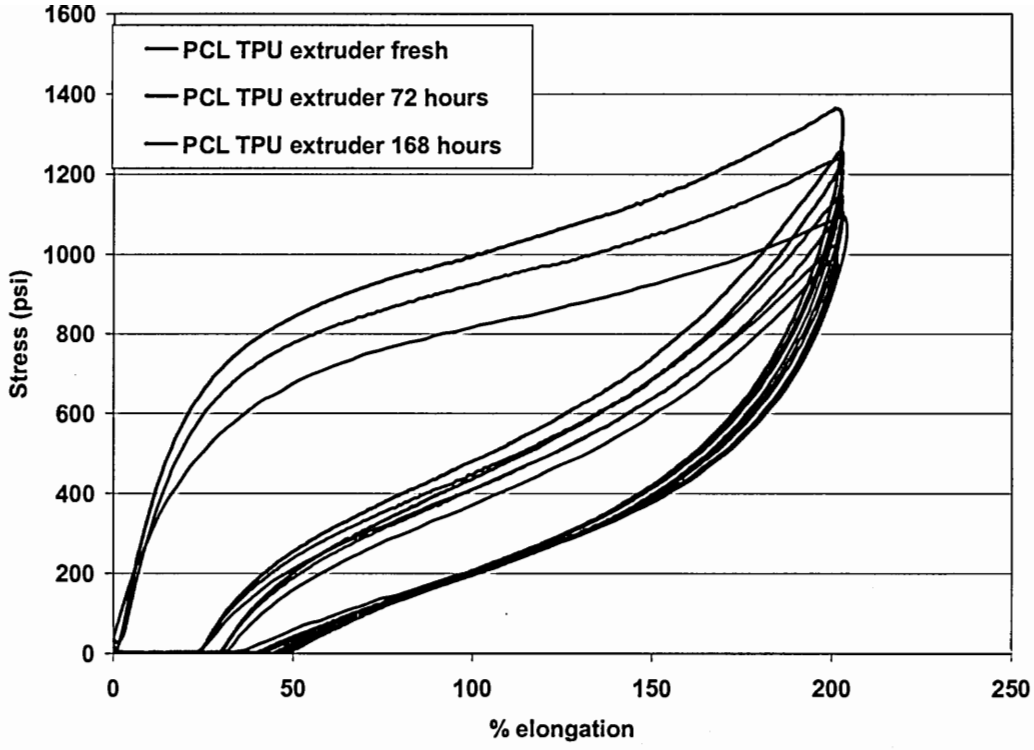

Figure 48. 200% elongation three cycle hysteresis test curves for the PCL TPU collected on a room temperature roll and tested fresh, at 72 hours and 1 week of age.

Tables 12 and 13 summarize the material parameters obtained from the hysteresis measurements of these polymers. These tables, and the graph shown in Figure 49, indicate that the magnitude of hysteresis decreases as a function of time as one would expect from a system that is undergoing phase segregation. One could also see from these figures that the elastomers reach equilibrium hysteresis behavior as quickly as the second cycle. Similar analysis of the PCL TPU data indicates that this polymer is an inferior elastic polymer. It has a larger hysteresis and set after cyclic elongation. Like the PTMO TPU, the PCL TPU also attains hysteresis equilibrium with the second cycle.

The actual magnitude of the hysteresis, both on the first and the second cycle, is much higher for the PCL TPU. Figure 49 shows a plot of the hysteresis as a function of time for both polymers of this study. The hysteresis of the PTMO TPU decreases as a function of time while the PCL TPU shows no signs of increase or decrease. The samples that are freshly extruded show more scatter of data which signifies the non-equilibrium nature of the phase segregation process.

Table 12. Summary of 200% elongation Hysteresis data for PTMO TPU

position	age of sample	% hysteresis 1st cycle	% hysteresis 2nd cycle	Immed set % after 2nd cycle
Extruder	fresh	54	30	50
Extruder	1 hour	59		
Extruder	3 hour	62	36	41
Extruder	3 day	59	33	34
Extruder	7 day	50	29	32
chill roll	fresh	53	29	51
chill roll	1 hour	61	36	52
chill roll	3 hour	59	35	42
chill roll	24 hour	57	35	33
chill roll	3 day	56	32	36
chill roll	7 day	54	31	35

Table 13. Summary of 200% elongation hysteresis for the PCL TPU

position	age of sample	% hysteresis 1st cycle	% hysteresis 2nd cycle	immed set % after 2nd cycle
extruder	fresh	71	45	63
extruder	1 hour	70	46	60
extruder	3 hour	71	46	59
extruder	24 hour	73	49	52
extruder	3 day	71	46	49
extruder	7 day	71	45	47
chill roll	fresh	71	45	62
chill roll	1 hour			
chill roll	3 hour	70	45	55
chill roll	24 hour			
chill roll	3 day	71	45	48
chill roll	7 day	70	45	46

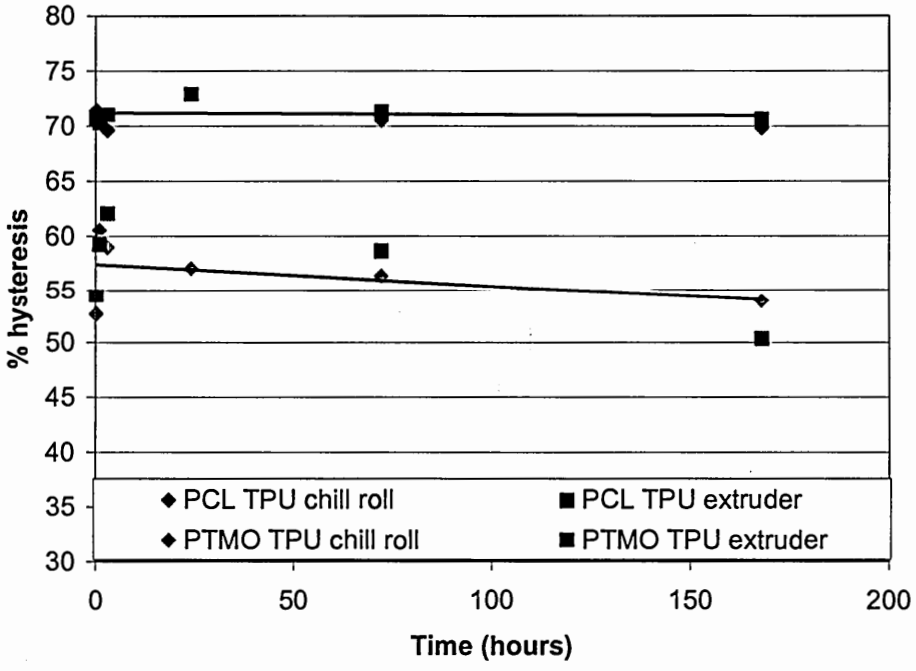

Figure 49. Percent hysteresis as a function of time from extrusion for the 2nd cycle of a three cycle 200% elongation hysteresis test.

An interesting property that showed an improvement in elastic property with time is the % set. Analysis of the plot shown in Figure 50 of the set as a function of time using a power law model indicates that the PTMO TPU phase segregates at a faster rate (slope = -0.07) than the PCL TPU (slope =-0.05). The PTMO TPU segregates two orders of magnitude faster than the PCL TPU system even at 40% lower hard segment content. Both the filaments collected on a chilled roll and a room temperature roll show a similar trend.

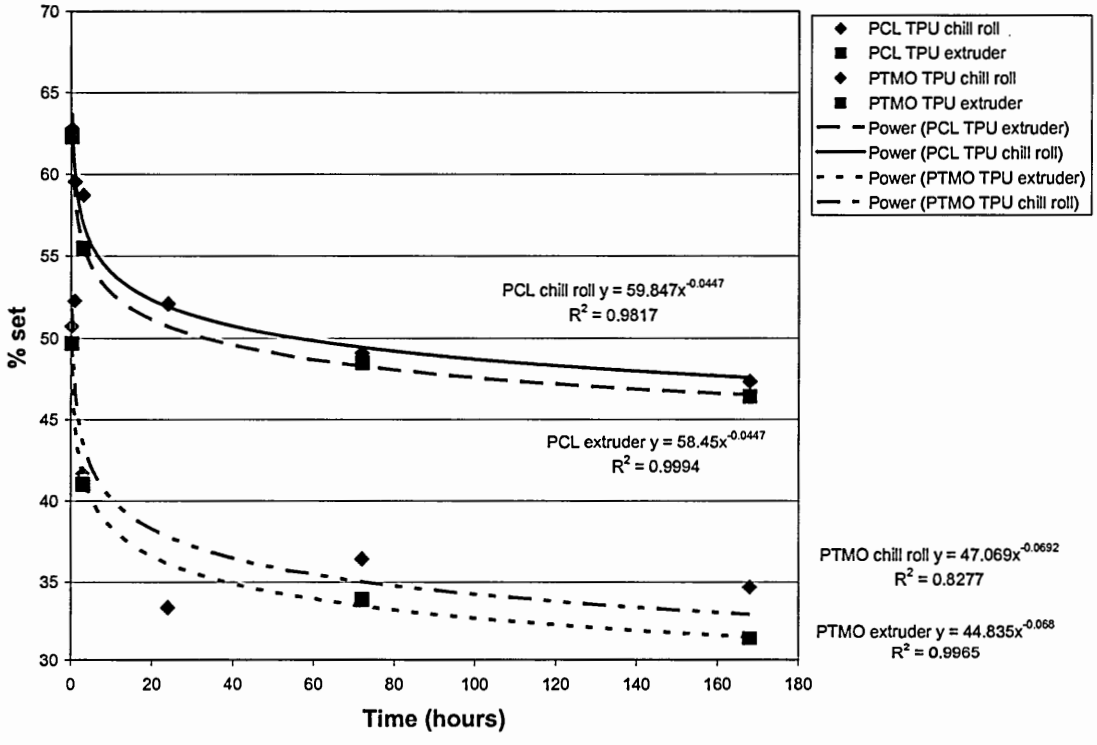

Figure 50. Chart of % set during the 200% elongation hysteresis test as a function of time from extrusion for the PCL and PTMO TPUs

One surprising outcome of this study is that the % set resulting from a hysteresis test correlates very well with the phase segregation seen with the SAXS results. This indicates that the phase segregation occurring on a molecular level is reflected in the set

data. As stated earlier, the validity of this approach must be confirmed by conducting more experiments

Thermal Behavior

Figures 51 and 52 show the DSC thermograms of the cast film and compressions molded equilibrium samples used in this study. These thermograms were obtained as a reference for comparison with the thermal behavior of the extruded and aged filaments generated at K-C and at BNL. Examination of the DSC thermogram shown in Figure 51 indicates that the PTMO TPU has several transitions. Figure 52 shows the DSC thermograms of the PCL based TPU. Tables 14 and 15 give the thermodynamic parameters associated with various phase transitions for these two polymers from analysis of the DSC curves below.

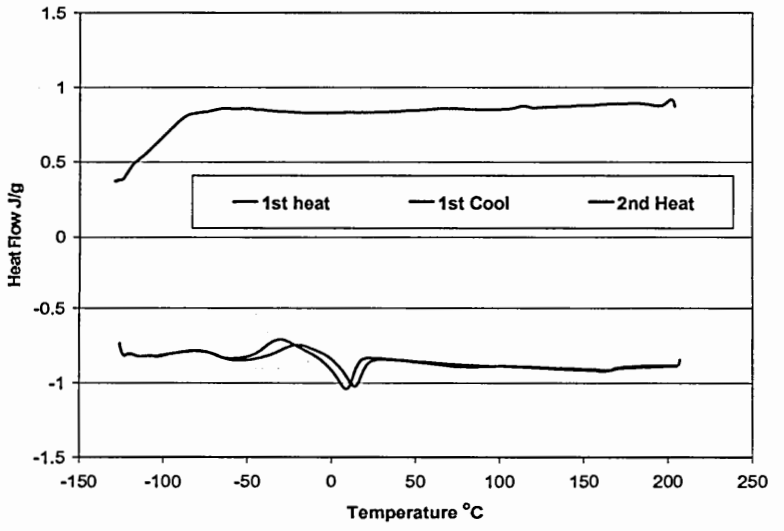

Figure 51. DSC thermogram of the PTMO TPU obtained from a solution-cast film at a heating and cooling rate of 10 °C/min in a nitrogen atmosphere.

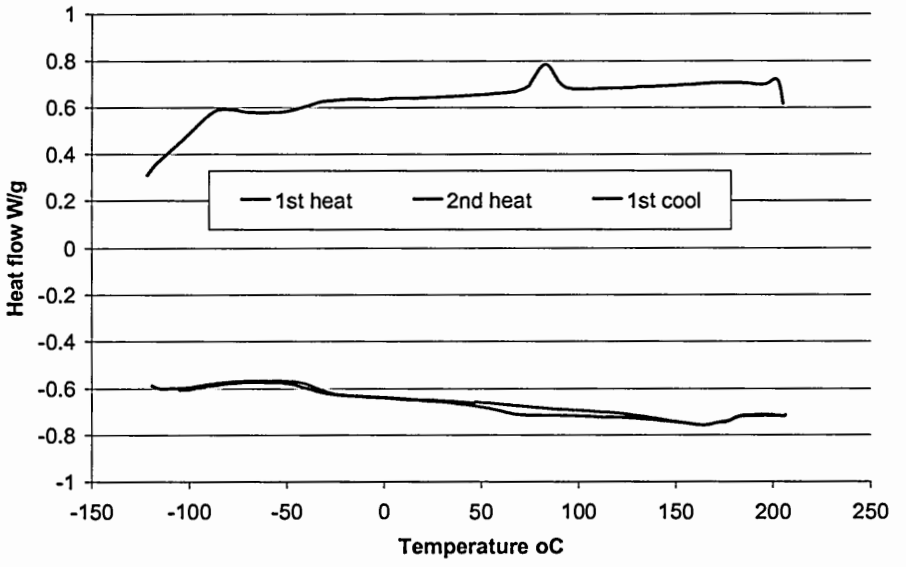

Figure 52. DSC thermogram of the PCL TPU obtained from a compression-molded film at a heating and cooling rate of 10 °C/min in a nitrogen atmosphere.

Table 14. DSC values of points of interest along thermograms for PTMO TPU generated from analysis of figure above

DSC	1^{st} T_g	delta C_p	1^{st} peak °C	cold cryst J/g	2^{nd} peak °C	melt J/g	difference J/g	3^{rd} peak °C	enthaply J/g
1st heat cycle	-67.8	-0.09	-30.2	11.2	8.8	10.5	0.72	164.9	0.63
1st cool cycle								113.2	0.40
2nd heat cycle	-69.6	-0.10	-20.2	10.6	13.8	8.2	2.46	160.8	0.59

Table 15. DSC values of points of interest along thermograms for PCL TPU generated from analysis of figure above

DSC	1^{st} T_g	delta C_p	2^{nd} T_g °C	delta C_p	peak max °C	enthalpy J/g
1st heat cycle	-46.3	-0.21	61.1	-0.23	164.7	10.0
1st cool cycle	-36.0	-0.21			82.7	12.2
2nd heat cycle	-34.6	-0.25			164.5	12.7

Thermal behavior of the PTMO TPU

The DSC thermograms of the PTMO TPU samples collected on a chilled roll as well as room temperature roll are shown in Figures 51 and 52. The thermograms were obtained only on the 1st heating cycle because it was important to know what has happened to the sample during the aging process. Once the sample is heated, it will change the thermal history and all the memory will be erased. Both Figures show strong resemblance to each other. The DSC curves are characterized with the soft segment glass transition at around -70°C, soft segment cold crystallization at approximately -25°C, a soft segment melting endotherm at about +10°C. There are two endothermic events which occur at around 70°C and 160°C. The peak at 70°C may be attributed to the association of moisture with the hard segment since the peak is absent in the second heating cycle of the equilibrated structure shown in Figure 51. The small peak at approximately 160°C most probably represents dissociation of partially ordered hard segments.

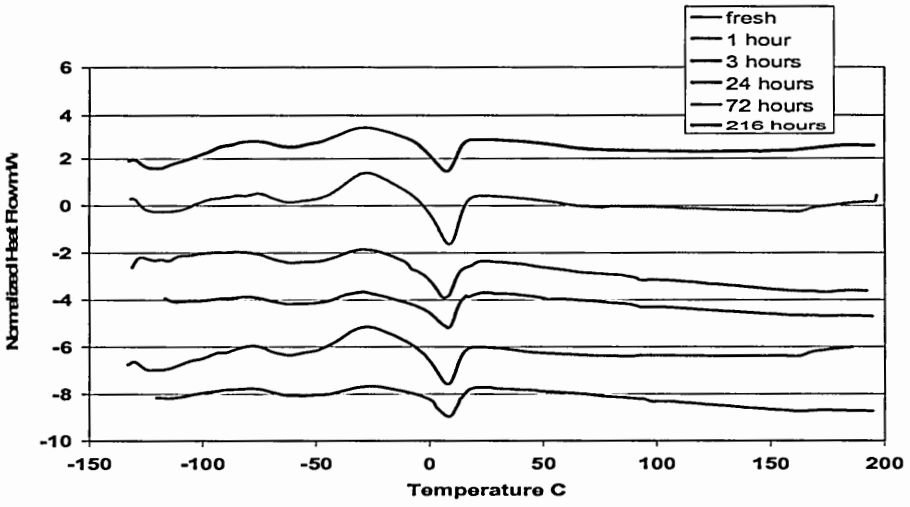

Figure 53. DSC 1st heat as a function of time for the PTMO TPU collected on a chilled roll

The glass transition temperature of the soft block and the enthalpy of melting did not show a consistent trend with aging time. Repetition of the experiments of the well aged samples showed significant scatter of the soft block glass transition temperature and melting endotherms. These results underline the difficulties of following the phase segregation through glass transition changes in these polymers which have a poor drive to phase segregate. This is supported by the data provided by SAXS studies where the morphology of the samples was found to be ill-defined.

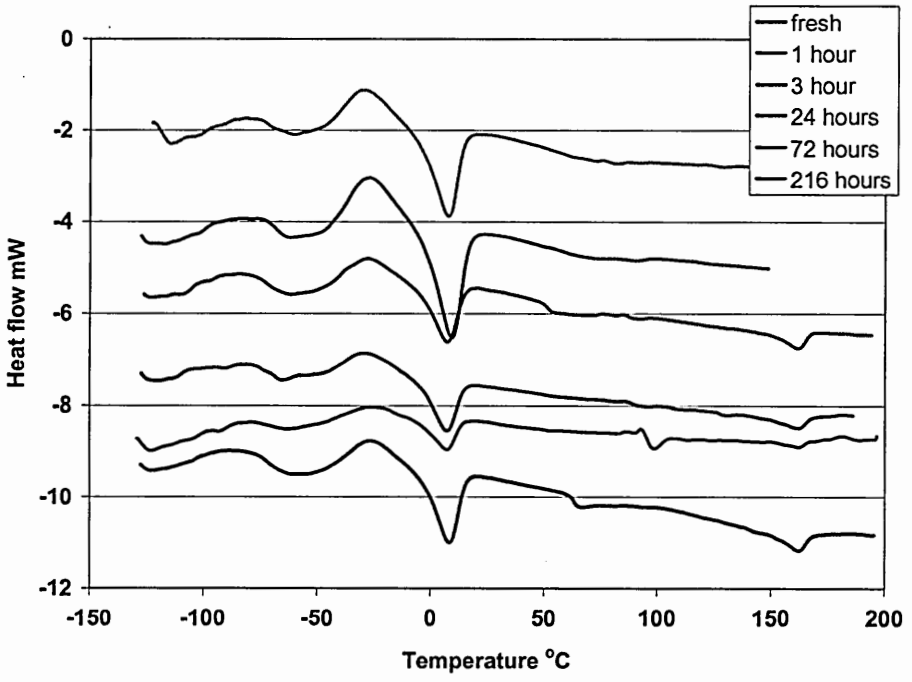

Figure 54. DSC 1st heat as a function of time for the PTMO TPU collected on a room temperature roll

Thermal Behavior of the PCL TPU system

The DSC thermograms of PCL TPU samples collected on a chilled roll are shown in Figure 55. As would be expected from the SAXS analysis, Figure 55 shows a very nondescript thermal profile due to the presence of domains with different sizes and different compositions. This same phenomenon was observed in a study by Chang, et al (1997) for TPUs with polyester soft segment type.[26] They attributed this DSC shape to both phase mixing and the existence of hydrogen bonding among the hard segments. However, comparison of this thermogram with one obtained for an equilibrated structure shown in Figure 52 on the 1st heat indicates that they both show similar behavior, i.e., a glass transition around -60°C and an endotherm around 65°C followed by a melting peak around 169°C. These figures indicate that the domain structure of the PCL TPU samples, as is the case of the PTMO TPU, is rather inhomogeneous. This is further supported by the data presented and discussed in the SAXS section.

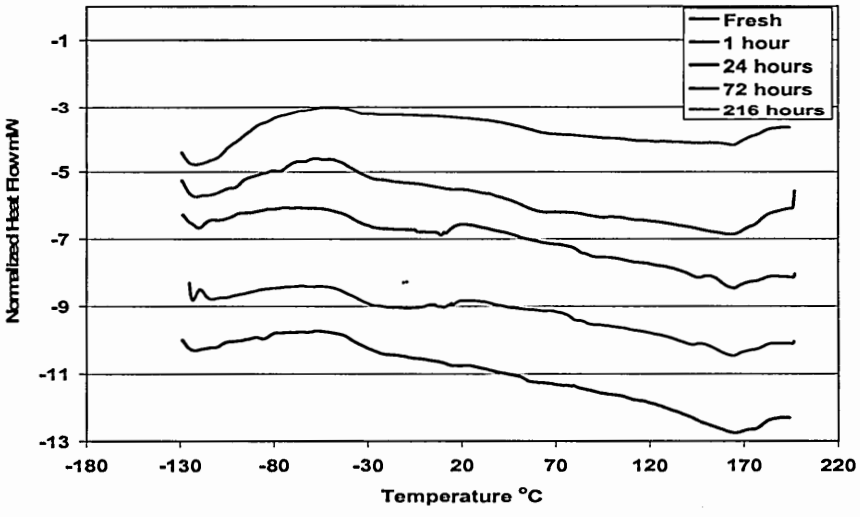

Figure 55. DSC 1st heat as a function of time for PCL TPU collected on a chilled roll

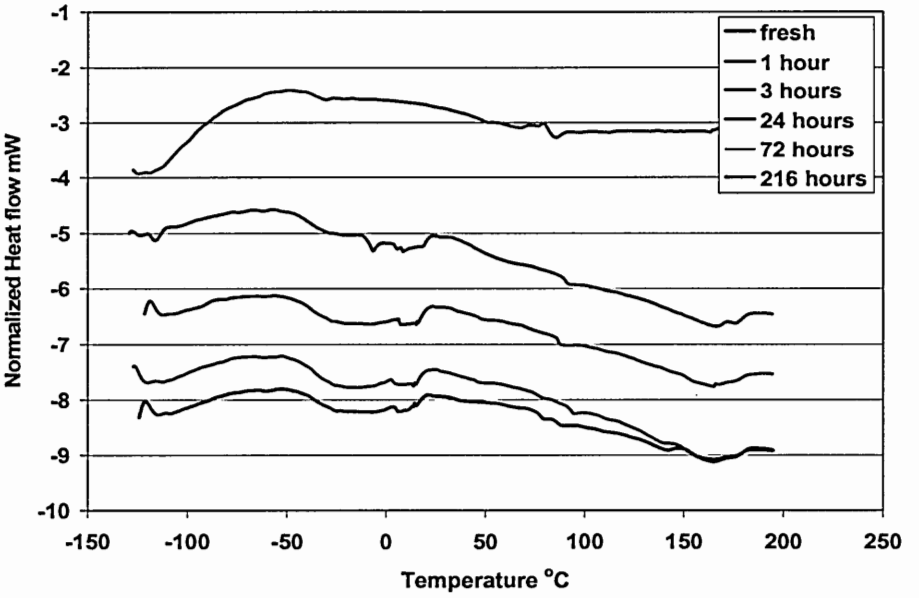

Figure 56. DSC 1st heat as a function of time for PCL TPU collected on a room temperature roll

The thermograms of the samples collected on a room temperature roll given in Figure 56 show a similar pattern to the samples collected on a chilled roll. The discussions presented above concerning the samples collected on a chilled roll are valid in this case as well.

CONCLUSIONS

The TPU polymers studied in this work show a poor tendency to phase segregate. This may be due to the commercial polymerization process used to produce the TPUs. A one shot process is used where the polyol soft segment, BDO, and MDI are mixed in one step. This process results in a broad distribution of hard segment sizes. The compatibility of the hard and soft segments combined with the distribution of the hard segment sizes promotes a phase mixed system. The PTMO TPU has a higher drive to phase segregate than the PCL TPU because of the chemical incompatibility of the hard and soft segments. Changes in the extruding roll temperature did not increase the level of order seen in the morphology of the two TPUs. Even at only 25% hard segment, the PTMO TPU has a higher drive to phase segregate than the PCL TPU at 39% hard segment. The added difference of a higher soft segment T_g for the PCL TPU further reduced the phase segregation kinetics for that system. The two TPUs have the same molecular weight.[13] It can be concluded that the PTMO TPU has a greater tendency to phase segregate due to thermodynamic and kinetic reasons. However, both the PTMO and PCL TPU systems show a weak tendency to phase segregate compared to styrenic block copolymers.

Evolution of the domain structure in the first few seconds after extrusion of the segregation process was studied by SAXS and modeled using the Debye approach. This analysis suggests that the domains are ill defined and random in size. As time progressed the systems could no longer be modeled using the Debye approach. The

Vonk 1-D correlation model was used successfully at longer times, indicating that some level of spacial order was present in the domain structure.

The SAXS approach to monitoring the phase segregation behavior worked best of all of the methods used in this study. DSC, DMTA, and stress elongation measurements could not differentiate between the subtle levels in the phase segregation across time. However, the % immediate set generated after the hysteresis cycle test did show a trend of better performance in samples with higher degrees of phase segregation. This result is slightly surprising and further testing of this approach should be explored to validate the observed correlation.

The PTMO TPU showed good properties and good processability. Recommendations for assessment will be made in film extrusion processes. Both TPUs processed well and could provide opportunities for development of alternate materials such as a component or layer in a film.

Better TPU phase segregation is expected in a copolymer with a higher thermodynamic drive to separate combined with a lower T_g soft segment system. The balance of soft stretch and % hard segment is crucial because an increase in the % hard segment will add to the thermodynamic drive to segregate but will also increase the hardness of the polymer creating too stiff a material for this application. The change in % hard segment may also change the viscosity of the system thus reducing the kinetic ability to phase segregate. Further analysis of TPU systems is planned with comparisons of different soft segments and assessments of processing methods. Plans are to evaluate TPUs without the combination of the MDI hard segment with an ester soft segment to drive thermodynamic incompatibility as far as possible. The cost

balance of the cheaper ester based soft segment with an alternate hard segment will also be assessed. The butane diol chain extender used in this study did not increase the thermodynamic drive to separate for the hard and soft segments; perhaps another chain extender such as an amine could be used. Soft segments with lower glass transition temperatures will also be looked for based on the learning of this study.

REFERENCES

1. C. Hepburn, "Polyurethane Elastomers", Applied Science Publishers, London, 1982.

2. N.R. Legge, G. Holden, H.E. Schroeder, "Thermoplastic Elastomers- A Comprehensive Review", Oxford University Press, New York, 1987.

3. United States Patent # 5,385,775

4. Chu et al.,"Synchrotron Studies of the Phase Separation Kinetics of a Segmented Polyurethane", Macromolecules 1992, 25, pp 1737-1742.

5. Chu et al.,"Multiphase Structure of Segmented Polyurethanes: Effect of Hard Segment Flexibility", Macromolecules 1993, 26, pp 612-622.

6. F.J. Balta-Calleja and C. G. Vonk,"X-Ray Scattering of Synthetic Polymers," Elsevier, New York (1989).

7. M. Kakudo and W. Kasai, "X-ray diffraction by polymers", Elsevier, New York, pp18 (1972).

8. Cooper et al, "Microphase Separation and Rheological Properties of Polyurethane melts I. Effect of Block Length", Macromolecules 1998, 31. pp 9181-9192.

9. Koberstein et al." Compression Molded Polyurethane Block Copolymers 2. Evaluation of Microphase Compositions", Macromolecules 1992, 25.pp 6205-6213.

10. Pompe et al, "Influence of processing conditions on the multiphase structure of segmented polyurethanes", Polymer 1998 Vol 39 No 21 pp 5147-5153.

11. Koberstein et al." Compression Molded Polyurethane Block Copolymer 1. Microdomain Morphology and Thermomechanical Properties" Macromolecules 1992, 25 pp 6195-6204.

12. Harrell et al. "Segmented Polyurethanes. Properties as a function of Segment size and Distribution", Macromolecules Vol 2 No6 November-December 1969 pp 607-612.

13. Private conversations with Dow Chemical Corporation, Gary Mistry.

14. Presentation by Ben Hsaio to Kimberly Clark Corp. 2001

15. Chu et al.,"In-Situ Synchrotron WAXD/SAXS Studies of Structural Development during PBO/PPA Solution Spinning", Macromolecules 2002, 35,pp 433-439.

16. A. Guinier and G. Ournet, "Small Angle X-Ray Scattering of X-rays," John Wiley and sons, Inc., New York (1955).

17. G. Porod, Kolloid-Z, 124(2), 83 (1951).

18. G. Porod, Kolloid-Z, 125(1), 51 (1952).

19. G. Porod, Kolloid-Z, 125(2), 108 (1952).

20. A. H. Compton and S.K. Allison, "X-Rays in Theory and Experiment," D. Van Nostrand Co., Inc., New York, 116ff (1935).

21. M. Kakudo and N. Kasai, "X-Ray Diffraction by Polymers", Elsevier Publishing Co., New York (1972).

22. Tyagi et al, "Small Angle X-Ray Studies of Siloxane-Urea Segmented Copolymers" Polymer Engineering and Science, mid-November 1986 Vol 26 No. 20 pp1371-1398.

23. D.W. Van Krevelen," Properties of Polymers", Elsevier, New York, (1990), pp 200-214.

24. G. Strobl, " The Physics of Polymers", Springer-Verlag, New York (1996).

25. Sauer et al., "Tapping Mode AFM Studies Using Phase Detection for Resolution of Nanophases in Segmented Polyurethanes and Other Block Copolymers" Macromolecules 1997, 30 pp 8314-8317.

26. Yu et al.,"Effect of side-chains on the phase segregation of polyurethanes using small angle X-ray scattering" Polymer Vol. 39, No. 15 1998 pp 3479-3489.

Appendix A

Table 1. Example of statistical results for Hysteresis testing of samples

soft segment	experimental date	position	age of sample	% hysteresis 1st cycle	% hysteresis 2nd cycle	immed set %
PCL	4/17/2003	extruder	fresh	70.70	45.10	62.95
				70.60	44.80	62.61
				70.60	44.90	62.78
			Average	70.63	44.93	62.78
			Stand. Dev	0.06	0.15	0.17
PCL	3/19/2003	extruder	3 hour	70.70	46.30	58.47
				71.40	46.20	58.95
				71.00	46.30	58.71
			Average	71.03	46.27	58.71
			Stand. Dev	0.35	0.06	0.24
PCL	3/19/2003	extruder	3 hour	69.60	44.70	55.83
				69.70	45.10	55.12
				69.60	44.90	55.48
			Average	69.63	44.90	55.48
			Stand. Dev	0.06	0.20	0.35
PCL	3/20/2003	extruder	24 hour	71.40	46.40	51.46
				74.40	50.70	52.70
				72.90	48.50	52.08
			Average	72.90	48.53	52.08
			Stand. Dev	1.50	2.15	0.62
PCL	3/22/2003	extruder	3 day	71.30	46.10	48.60
				71.20	46.40	49.50
				71.30	46.30	49.05
			Average	71.27	46.27	49.05
			Stand. Dev	0.06	0.15	0.45
PCL	3/26/2003	extruder	7 day	70.50	45.30	47.69
				70.80	45.10	46.92
				70.60	45.20	47.31
			Average	70.63	45.20	47.31
			Stand. Dev	0.15	0.10	0.38
PCL	4/17/2003	chill roll	fresh	70.80	45.10	61.78
				71.40	45.60	62.79
				71.10	45.30	62.28
			Average	71.10	45.33	62.28
			Stand. Dev	0.30	0.25	0.50
PCL	3/22/2003	chill roll	3 day	70.40	45.10	48.95
				70.60	45.20	47.98
				70.50	45.20	48.46
			Average	70.50	45.17	48.46
			Stand. Dev	0.10	0.06	0.48
PCL	3/26/2003	chill roll	7 day	69.60	44.50	45.91
				69.90	44.50	46.87
				69.80	44.50	46.39
			Average	69.77	44.50	46.39
			Stand. Dev	0.15	0.00	0.48

Table 1. Continued

PTMO	4/17/2003	Extruder	fresh	54.60	30.00	50.78
				54.20	29.90	48.51
				54.40	29.90	49.64
			Average	54.40	29.93	49.64
			Stand. Dev	0.20	0.06	1.13
PTMO	4/18/2003	Extruder	1 hour	59.40		7.78
				59.10		10.23
				59.20		9.00
			Average	59.23		9.00
			Stand. Dev	0.15		1.23
PTMO	3/22/2003	Extruder	3 day	60.40	32.90	35.29
				56.70	32.20	32.55
				58.60	32.50	33.92
			Average	58.57	32.53	33.92
			Stand. Dev	1.85	0.35	1.37
PTMO	3/26/2003	Extruder	7 day	50.30	28.40	31.22
				50.40	28.60	31.79
				50.30	28.50	31.51
			Average	50.33	28.50	31.51
			Stand. Dev	0.06	0.10	0.28
PTMO	4/17/2003	chill roll	fresh	52.70	28.70	51.97
				52.40	28.60	49.43
				52.60	28.60	50.70
			Average	52.57	28.63	50.70
			Stand. Dev	0.15	0.06	1.27
PTMO	3/19/2003	chill roll	fresh	60.20	35.50	51.00
				60.80	36.60	53.49
				60.50	36.00	52.24
			Average	60.50	36.03	52.24
			Stand. Dev	0.30	0.55	1.25
PTMO	3/19/2003	chill roll	1 hour	60.20	35.50	51.00
				60.80	36.60	53.49
				60.50	36.00	52.24
			Average	60.50	36.03	52.24
			Stand. Dev	0.30	0.55	1.25
PTMO	3/19/2003	chill roll	3 hour	58.90	35.10	39.76
				58.90	34.60	43.55
				58.90	34.80	41.65
			Average	58.90	34.83	41.65
			Stand. Dev	0.00	0.25	1.89
PTMO	5/18/2003	chill roll	24 hour	42.20	19.00	25.71
				43.90	20.20	22.53
				43.00	19.60	24.12
			Average	43.03	19.60	24.12
			Stand. Dev	0.85	0.60	1.59
PTMO	3/22/2003	chill roll	3 day	55.70	32.20	36.72
				56.90	32.10	36.08
				56.30	32.20	36.40
			Average	56.30	32.17	36.40
			Stand. Dev	0.60	0.06	0.32
PTMO	3/26/2003	chill roll	7 day	53.70	31.10	34.70
				53.90	31.00	34.60
				53.80	31.10	34.65
			Average	53.80	31.07	34.65
			Stand. Dev	0.10	0.06	0.05